Quaternary Science Reviews 299 (2023) 107867

Contents lists available at ScienceDirect

Quaternary Science Reviews

journal homepage: www.elsevier.com/locate/quascirev

A 1.8 million year history of Amazon vegetation

Andrea K. Kern [a, *], Thomas Kenji Akabane [b], Jaqueline Q. Ferreira [b], Cristiano M. Chiessi [c], Debra A. Willard [d], Fabricio Ferreira [e, f], Allan Oliveira Sanders [e, f], Cleverson G. Silva [e], Catherine Rigsby [g], Francisco W. Cruz [b], Gary S. Dwyer [a], Sherilyn C. Fritz [h], Paul A. Baker [a]

[a] Division of Earth and Ocean Sciences, Duke University, Durham, NC 27708, USA
[b] Department of Sedimentary and Environmental Geology, Institute of Geosciences, University of São Paulo, Rua do Lago 562, CEP: 05508-080, São Paulo, SP, Brazil
[c] School of Arts, Sciences and Humanities, University of São Paulo, Av. Arlindo Bettio 1000, CEP: 03828-000, São Paulo, SP, Brazil
[d] US Geological Survey, 926A National Center, Reston, VA 20192, USA
[e] Marine Geology Laboratory (LAGEMAR), Institute of Geosciences, Universidade Federal Fluminense, Av. Gal. Milton Tavares de Souza s/n, CEP: 24210-346, Niterói, RJ, Brazil
[f] Postgraduate Program in Ocean and Earth Dynamics, Institute of Geosciences, Universidade Federal Fluminense, Av. Gal. Milton Tavares de Souza s/n, CEP: 24210-346, Niterói, RJ, Brazil
[g] Department of Geological Sciences, East Carolina University, Greenville, NC 27858, USA
[h] Department of Earth and Atmospheric Sciences, School of Biological Sciences, University of Nebraska – Lincoln, Lincoln, NE 65588, USA

ARTICLE INFO

Article history:
Received 25 August 2022
Received in revised form
24 October 2022
Accepted 5 November 2022
Available online 26 November 2022

Handling Editor: Dr I Hendy

Keywords:
Biodiversity
Vegetation
Palynology
Mid-pleistocene transition
Glacial-interglacial cycles
South America

ABSTRACT

During the Pleistocene, long-term trends in global climate were controlled by orbital cycles leading to high amplitude glacial-interglacial variability. The history of Amazonian vegetation during this period is largely unknown since no continuous record from the lowland basin extends significantly beyond the last glacial stage. Here we present a paleoenvironmental record spanning the last 1800 kyr based on palynological data, biome reconstructions, and biodiversity metrics from a marine sediment core that preserves a continuous archive of sediments from the Amazon River.

Tropical rainforests dominated the Amazonian lowlands during the last 1800 ka interchanging with surrounding warm-temperate rainforests and tropical seasonal forests. Between 1800 and 1000 ka, rainforest biomes were present in the Amazon drainage basin, along with extensive riparian wetland vegetation. Tropical rainforest expansion occurred during the relatively warm Marine Isotope Stages 33 and 31 (ca. 1110 to 1060 ka), followed by a contraction of both forests and wetlands until ca. 800 ka. Between 800 and 400 ka, low pollen concentration and low diversity of palynological assemblages renders difficult the interpretation of Amazonian vegetation. A strong synchronicity between vegetation changes and glacial-interglacial global climate cycles was established around 400 ka. After 400 ka, interglacial vegetation was dominated by lowland tropical rainforest in association with warmer temperatures and higher CO_2. During cooler temperatures and lower CO_2 of glacial stages, tropical seasonal forests expanded, presumably towards eastern Amazonia. While this study provides no evidence supporting a significant expansion of savanna or steppe vegetation within the Amazonian lowlands during glacial periods, there were changes in the rainforest composition in some parts of the basin towards a higher proportion of deciduous elements, pointing to less humid conditions and/or greater seasonality of precipitation. Nevertheless, rainforest persisted during both glacial and interglacial periods. These findings confirm the sensitivity of tropical lowland vegetation to changes in CO_2, temperature, and moisture availability and the most suitable conditions for tropical rainforests occurred during the warmest stages of the Mid Pleistocene Transition and during the interglacial stages of the past 400 kyr.

1. Introduction

The Mid-Pleistocene Transition (~1250–700 ka; MPT; Clark et al., 2006) represents a major climate interval of the

* Corresponding author.
E-mail address: annkkern@gmail.com (A.K. Kern).

https://doi.org/10.1016/j.quascirev.2022.107867
0277-3791/

Pleistocene, marking a shift from lower-amplitude, high frequency, obliquity driven ~41 kyr glacial-interglacial cycles to a high-amplitude, lower frequency, eccentricity-driven periodicity of ~100 kyr (Mudelsee and Schulz, 1997). Following the MPT, interglacial stages attained higher temperatures and atmospheric CO_2 levels than previously, whereas the glacial stages of the late Pleistocene became far colder with lower atmospheric CO_2 levels (Lisiecki and Raymo, 2005; Chalk et al., 2017; Berends et al., 2021). These resulted in changes of ice sheet dynamics, glacial ice volume, sea ice extent, eustatic sea level, and ocean and atmospheric meridional heat transport (Clark et al., 2006, 2017; Bell et al., 2015; Willeit et al., 2019), and in turn had a major impact on the nature and composition of global ecosystems (Dupont et al., 2001; Oliveira et al., 2017).

However, continuous records of the dynamics of terrestrial biota and ecosystems during this period are limited (e.g., Torres et al., 2013; Tarasov et al., 2013; Hooghiemstra et al., 2022). Particularly in the tropics, Pleistocene records of environmental change are rare, including Amazonia, the region with the highest biodiversity on Earth (da Silva et al., 2005; Rull, 2011). To date, only one archive from the high tropical Andes (yet outside the bounds of the Amazon drainage basin) continuously describes vegetation dynamics beyond 1 Ma (Hooghiemstra, 1984; Torres et al., 2013). Pleistocene paleoenvironmental records are also not well resolved in the longest marine palynological studies of Amazonian history (e.g. Hoorn et al., 2017). Among continental records from the Amazonian lowlands, there are few vegetation and climate records covering more than one glacial-interglacial cycle (Absy et al., 1991; Hermanowski et al., 2012). As a result of the limited number of pollen records, many open questions on past glacial vegetation in Amazonia remain, even for the most recent glacial stage, the Last Glacial Maximum (LGM, 26.50–19 ka; Clark et al., 2009).

Haffer's (1969) Pleistocene Refugia hypothesis, which postulated an expansion of savannas that acted as both a barrier for tropical forest species and a driver of biodiversity, catalyzed interest in studies about the late Pleistocene environments of Amazonia. Many subsequent palynological, geochemical, and modelling studies have arrived at divergent conclusions (e.g., van der Hammen, 1974; van der Hammen and Absy, 1994; Colinvaux et al., 1996, 2000; Ledru et al., 1998; D'Apolito et al., 2013; van der Hammen and Hoogiehmstra, 2000). Drier-than-modern conditions for the LGM have been suggested for eastern Amazonia (Häggi et al., 2017; Wang et al., 2017) where vegetation modelling studies suggest potential for biome turnover under low CO_2 and increased fire activity (Sato et al., 2021; Maksic et al., 2022). Yet, overall proxy records remain ambiguous concerning both the magnitude of decreased humidity and extent of the increased openness of rainforest vegetation in different parts of Amazonia across glacial-interglacial intervals of the Pleistocene (e.g. Colinvaux et al., 2000; Baker and Fritz, 2015; Wang et al., 2017; Reis et al., 2017; Baker et al., 2020).

Here, we present a new pollen-based record from marine sediment core CDH-79 collected from the top of a seamount in the western equatorial Atlantic immediately adjacent to the Amazon continental margin (Fig. 1; 2). The record spans the last 1.80 Ma (Ferreira et al., 2021) and represents the longest and most continuous Quaternary vegetation reconstruction for the Amazon Basin. By reconstructing affinities of all biomes within the Amazon drainage basin following Marchant et al. (2009), we document the history of Amazonian biomes (Fig. 1B) and the impact of global climate and CO_2 change on prevailing vegetation types. In addition, we analyze patterns of Amazonian biodiversity by calculating specific metrics to identify significant vegetation variations and turnovers through time.

2. Regional setting

2.1. Vegetation types in the Amazonian drainage basin

The Amazonian drainage basin covers a large area with various vegetation types. The vegetation types of tropical South America are strongly affected by large gradients in elevation (to >6000 m; Fig. 1A) and precipitation (Burnham and Graham, 1999; Daly and Mitchell, 2000). It remains challenging to classify the vegetation on a continental scale, considering the high heterogeneity of certain vegetation types, their often disjunct areas, and varying classification of local vegetation (Pires and Prance, 1985; Daly and Mitchell, 2000). Several concepts have been developed to describe the vegetation types of tropical South America and inside the Amazonian drainage basin, but the number, size, and extent of single biomes still varies depending on source information and focus. In this context, the term “biome” represents a physiognomic vegetation unit established on a global scale, which is defined by plant traits and climate (Prentice et al., 1992; Marchant et al., 2009). Biomes are one basis to establish ecoregions, which additionally recognize distinct assemblages of natural communities and species to set boundaries (Olson et al., 2001, Fig. 1B).

The main biome of the modern Amazon drainage basin (Fig. 1B) is the evergreen moist tropical rainforest known as the Amazonian rainforest (tropical rainforest; TRFO; Marchant et al., 2009, Table 1), part of the tropical and subtropical moist broadleaved forest (Olson et al., 2001, Fig. 1B). It is characterized by a predominantly closed canopy with emergent trees and structured layers in the subcanopy, intolerant to fire and frost (Daly and Mitchell, 2000; Marchant et al., 2009). In certain areas, it extends to altitudes as high as 1000 m (Furley, 2007).

Open vegetation types in the lowlands of the Amazonian drainage basin (Fig. 1B) include the surrounding savannas (e.g. Cerrado, Guyannas, Llanos de Moxos) and edaphically constrained enclaves such as the campinaranas (Fig. 1B) (Pennington et al., 2000; Furley, 2007). The Cerrado occupies a large portion of southeastern Amazon basin (Fig. 1B) and is a mosaic of vegetation types varying in its openness between grass-dominated vegetation, woodlands and open forests (Eiten, 1972; Werneck, 2011) classifiying as tropical and subtropical grasslands, savannas and shrublands according to Olson et al. (2001, Fig. 1B). While climate, fire, and topography define the extent of the Cerrado, nutrient-poor and aluminum-rich soils also play a significant role in its distribution (Daly and Mitchell, 2000; Oliveira and Marquis, 2002; Werneck, 2011). Further, water storage capacity and soil-moisture determine the height and density of the woody elements (Furley, 2007). According to the classification of vegetation biomes used in Marchant et al. (2009), there is no single biome to represent the modern Cerrado. This vegetation tyoe is split into its woody component, merged in the Tropical Dry Forest (TDFO), and its grass and herbaceous dominated component which is included in the steppe biome (STEP) (Table 1; Supplementary Table 2).

A transitional biome between the evergreen moist tropical forest and the tropical dry forest is the Tropical Seasonal Forest (TSFO) as classified by Marchant et al. (2009), although no distinction was made by Olson et al. (2001; Fig. 1B). The TSFO represents a forest characterized by a mix of evergreen and sclerophyllous elements (“Cerrado elements”), comparable to the Mato Grosso seasonal forest (Fig. 1B) (Daly and Mitchell, 2000). During most of the year, the TSFO has a closed canopy with vegetation structure similar to the tropical rainforest, which only opens during the short dry season when the deciduous taxa shed their leaves. Therefore, some refer to this biome as semi-deciduous forests (e.g. Daly and Mitchell, 2000). Within the Amazon basin, the modern TSFO only

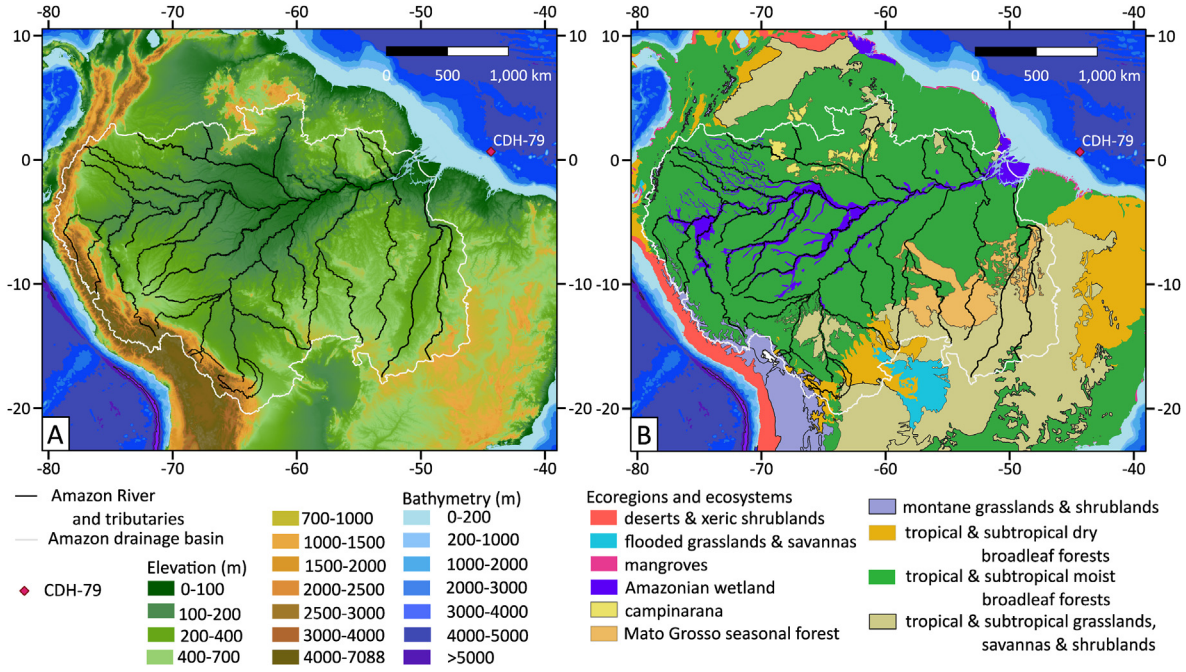

Fig. 1. A: Digital Elevation Model of the Amazon drainage basin and the location of core site CDH-79; B: Ecoregions of the Amazon drainage basin following Olson et al. (2001); selected WFF terrestrial ecosystems were added including the azonal wetland (várzea and igapó) ecosystems along the Amazon River and its catchment; the campinarana vegetation (white-sand vegetation) in the northernmost Amazon basin and the Mato Grosso seasonal forest. Cerrado vegetation is part of the tropical and subtropical grasslands, savannas and shrublands whereas páramo and puna are integrated in the montane grasslands and shrublands. Additional local vegetation classifications of each biome are listed in Table 1. The location of site CDH-79 is also shown.

Table 1
Overview of the main biomes within the Amazonian drainage basin today along with their abbreviations and main information summarized from Marchant et al. (2009).

Code	Biome name	Description	Additional information
TRFO	Tropical rainforest	Closed canopy lowland evergreen forest, precipitation >1500 mm, frost-intolerant	Amazonian rainforest known as *terra firme* forest including coastal mangrove vegetation
TSFO	Tropical seasonal forest	Closed canopy forest with deciduous elements, seasonally dry (1–4 months)	Mixed of mesophyllous and sclerophyllous taxa, mainly savanna gallery forest and seasonal swamp forest
TDFO	Tropical dry forest	Mixed forest, longer dry season than in the TSFO leads to drought and high water stress	Xerophytic vegetation types such as Andean xerophytic bush, Rupununi savanna, *cerrado*, *cerradão*, *campos rupestres*, *campo cerrado*, cactus forest, deciduous xerophytic forest, *campina*, *campinarana*, restinga, dune forest
WTRF	Warm temperate rainforest	Lower evergreen closed forest with trees >20 m, transitional forest type (1000–2500 m), frost-intolerant	(Moist) lower montane forest with a mix of mesophyllous and sclerophyllous elements, also referred to as submontane or evergreen premontane rainforest and evergreen lower montane forest
WEFO	Warm temperate evergreen broadleaf forest	Evergreen, semi-closed forest, frost-intolerant	Transitional and upper Andean forest (1000–2000 m) similar to the WTRF in higher elevation, not present in the eastern Brazilian highlands
COMI	Cool mixed forest	Low woodlands (<5 m) with an open canopy, frost-tolerant (night frosts)	High Andean forest with mainly evergreen elements; upper montane forest
CGSH	Cool grass- and shrubland	Tropical-alpine environment above the forest line in the Andes	Poaceae-dominated cool grassland with shrubby/woody vegetation like *páramo* and *subpáramo*
CGSS	Cool grasslands	High Andean grassland with tussock grasses and cushion plants	Poaceae-dominated cool grassland or heath, including *puna*, cushion *páramo* and super-*páramo*
STEP	Steppe	Dominated by grasses with shrubs and herbs	Warm grasslands of mainly Poaceae and Amaranthaceae in NE Brazil, including *campo limpo*, *caatinga* type *seridó*

occupies patches near the Guianas and at the southern margins of the Amazonian rainforest (Daly and Mitchell, 2000; Furley, 2007).

Montane and submontane forests in the Amazonian drainage basin are found on the Guiana and Brazilian Shields and in the Andes (Fig. 1B). Generally, as altitude increases, diversity and height of the vegetation gradually decrease (Homeier et al., 2008 and references therein), favoring the presence of herbs and shrubs at higher elevations (Daly and Mitchell, 2000). A low-elevation forest with a high biodiversity persists up to ca. 1500 m and shares many elements with lowland forest (Pérez-Escobar et al., 2021). Marchant et al. (2009) define several altitudinal forest biomes, based on an increasing number of montane elements. The lowest, warm temperate rainforest (WTFO) and the warm temperate evergreen broadleaf forest (WEFO), are both frost intolerant and occur up to an elevation of 2000 m. The upper montane forests are distinguished by the regular occurrence of night frosts (Pérez-Escobar et al., 2021) and by small trees (<10 m). One type is the cool mixed forest (COMI; Marchant et al., 2009) whereas cooler forest types such as the cold temperate rainforest (CTRF; Marchant et al., 2009) are not present within the Amazon drainage basin today. At the edges of the Amazonian drainage basin, two tropical alpine grass-dominated biomes occur in the high Andes (Fig. 1B),

commonly referred to as páramo and puna (Cuatrecasas, 1958; Halloy et al., 2008). Plants of both vegetation types are adapted to frost and occur at elevations between forest line and permanent snow cover (Londoño et al., 2014). Due to its higher precipitation (1000–3000 mm annually), the páramo is characterized by common presence of shrubs and dwarf trees, which are almost absent in the arid puna (Halloy et al., 2008). In both vegetation types, higher density of cushion plants occur with increasing elevation at the expense of decreasing grass abundances (Halloy et al., 2008; Londoño et al., 2014). Marchant et al. (2009) also distinguishes two high alpine grassland biomes. These mainly differ due to the presence of cushion plants associated with the cool grasslands (CGSS) while the cool grass- and shrubland (CGSH) has an additional component of dwarf trees and shrubs. A summary of all biomes and their abbreviations within the Amazonian drainage basin is listed in Table 1 and further includes regionally-used names of vegetation types.

2.2. Ocean currents in the western equatorial Atlantic

The material studied herin originates from a marine core labelled CDH-79, which was collected in a seamount in the equatorial western Atlantic. The upper water column surrounding the site CDH-79 is occupied by the North Brazil Current (NBC; Fig. 2A), a warm surface current that flows northwestwards along the northeastern South American continental margin (Peterson and Stramma, 1991). The NBC has two main roles in the global ocean—it is part of the wind-driven equatorial Atlantic gyral circulation, and it feeds the northward cross-equatorial current that balances the deep, southward-flowing North Atlantic Deep Water, both being important portions of the Atlantic Meridional Overturning Circulation (AMOC) (Fratantoni et al., 2000; Buckley and Marshall, 2016). By virtue of its dual roles, it is likely that the NBC has been present along the equatorial margin of South America since the establishment of AMOC and Atlantic equatorial ocean gyres (Nilsson et al., 2013), but these histories are not well known. Further, the NBC transports the freshwater and terrigenous suspended sediment that are delivered to the mouth of the Amazon, as well as rivers of Northeastern Brazil (e.g. Tocantins, Parnaíba, Mearim, Acaraú, Grande do Norte rivers; Fig. 2A) (Lentz, 1995; Allison et al., 2000). A substantial portion of the Amazonian sediments sink in the water column along its way to the Caribbean and are deposited off northeastern South America (e.g. Govin et al., 2012; Häggi et al., 2016).

At greater water depth, between ca. 1200 and 4000 m, the Deep Western Boundary Current (DWBC) transports North Atlantic Deep Water southeastwards into the South Atlantic (Fig. 2B) (Molinari et al., 1992; Fischer and Schott, 1997; Richardson and Fratantoni, 1999). Importantly, the DWBC entrains and transports Amazonian sediments southeastwards (Petschick et al., 1996), controlling the small terrigenous sediment deposition at the seamount site of CDH-79 (Fig. 2B).

3. Material and methods

3.1. Site description and age model

Marine sediment core CDH-79 (00° 39.69′ N, 44° 20.77′ W; 32.20 m core length; 2345 m water depth) was retrieved from a seamount located 320 km off the modern coastline of northeastern Brazil in the western equatorial Atlantic during the oceanographic expedition R/V Knorr (KNR 197–4) in February 2010 (Fig. 2). Surrounding water depth averages 3100 m; thus, the seamount stands ~750 m above the seafloor, where it is largely unaffected by downslope bottom sedimentation and erosion.

The age model for CDH-79 is based on radiocarbon (^{14}C) ages, Quaternary planktonic foraminifera biostratigraphy (Ericson and Wollin, 1968; Wade et al., 2011), and stable oxygen isotopic analyses (δ^{18}O) (Ferreira et al., 2021). Oxygen isotopic analysis (Fig. 3A) were undertaken on planktonic foraminifera (*Globigerinoides ruber* (white) within the size fraction 250–350 μm and benthic foraminifera (*Uvigerina peregrina* and *Cibicidoides wuellerstorfi* within the size fraction >125 μm). Details regarding the age dating can be found in Ferreira et al. (2021). Sediment deposition was nearly continuous except for a depositional unconformity visible as a 2-cm-thin bed of sand at ~55 cm core depth between two biostratigraphic zones (Ferreira et al., 2021).

3.2. Neodymium isotopes

To determine the provenance of sediments of core CDH-79, the neodymium isotopic composition of 22 carbonate-free sediment

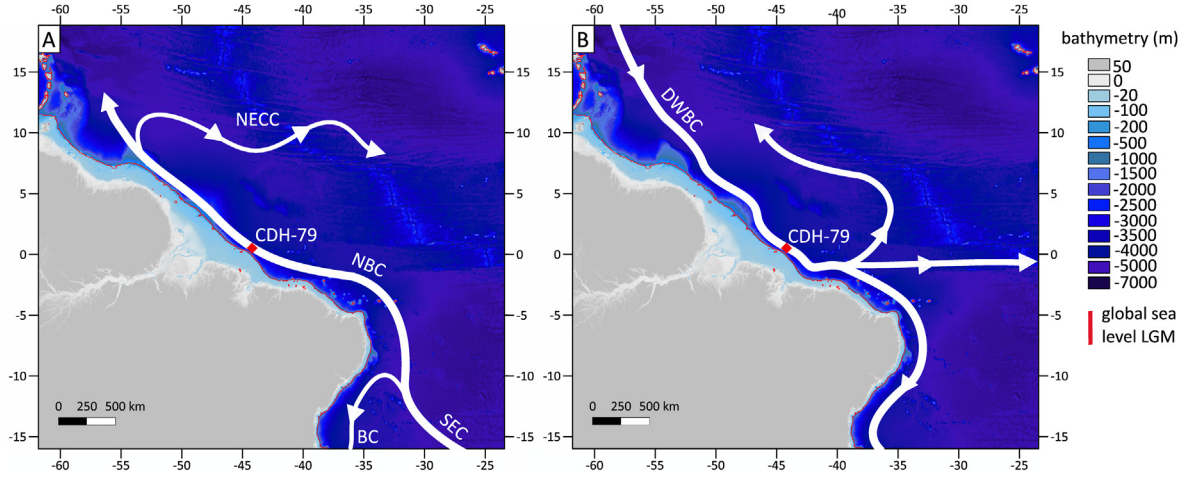

Fig. 2. Schematic map showing the main ocean currents in the equatorial western Atlantic affecting the sediment transport to site CDH-79. The red line represents the lower global eustatic sea level during the LGM based on CIMP5 (Abe-Ouchi et al., 2015) downscaled by woldclim (http://www.worldclim.com/). **A:** Surface currents following Peterson and Stramma (1991) and Richardson et al. (1994); BC: Brazil Current; NBC: North Brazil Current; NECC: North Equatorial Countercurrent; SEC: South Equatorial Current. **B:** Deep water currents following Stramma and England (1999) and Böning and Kröger (2005); DWBC: Deep Western Boundary Current. (For interpretation of the references to colour in this figure legend, the reader is referred to the Web version of this article.)

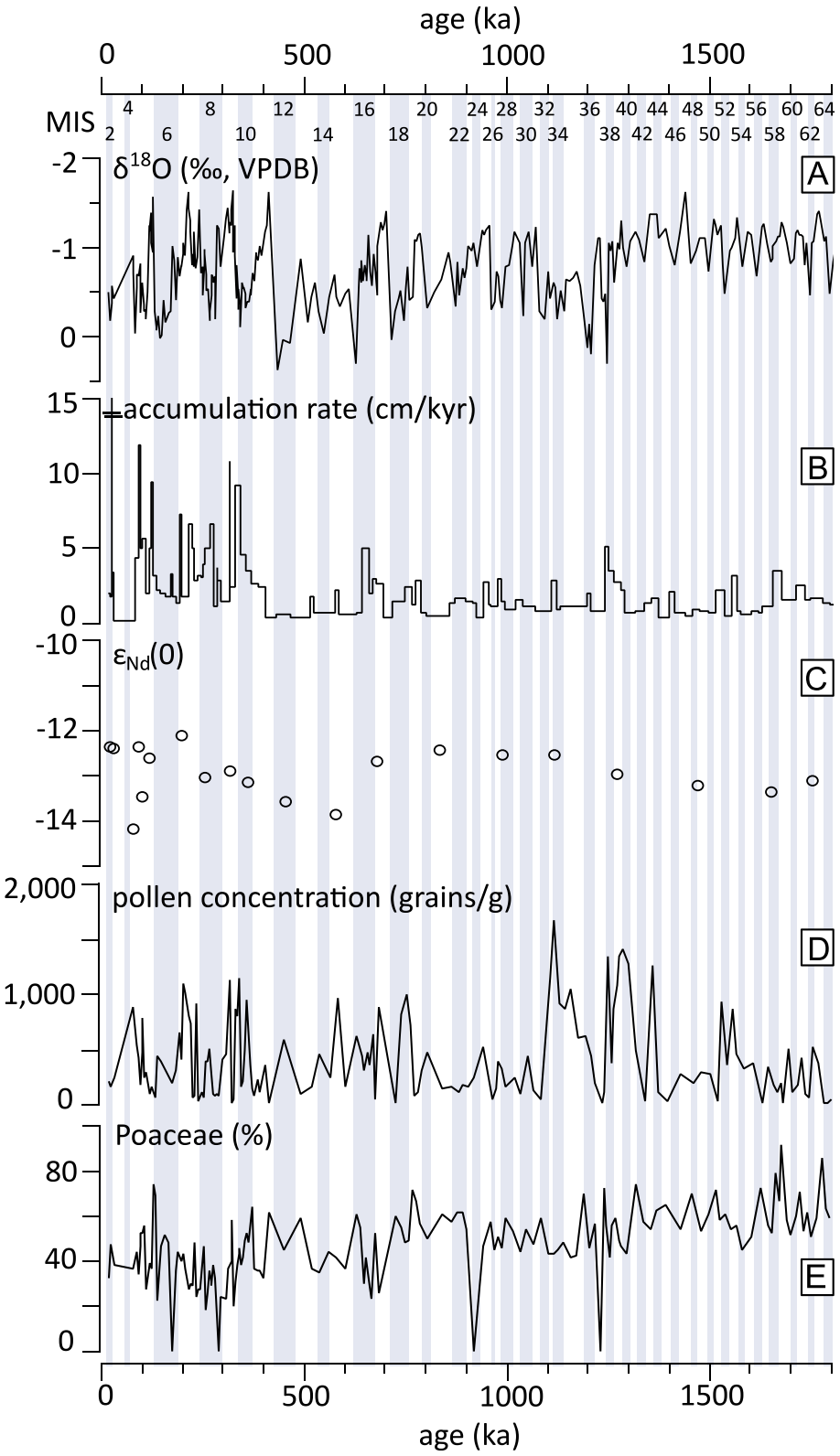

Fig. 3. Overview of various proxies from CDH-79 covering the last 1800 ka. Vertical grey bars indicate glacial stages, which are labelled on top of figure. A**:** Measured $\delta^{18}O$ ratios (Ferreira et al., 2021); **B:** accumulation rate calculated with the age model by Ferreira et al. (2021) with the highest peak, 26.44 to 26.35 ka, truncated; **C:** ε_{Nd} ratios measured on carbonate bulk-free samples; **D:** pollen concentration calculated as pollen grains per gram dry sediment for all palynological samples; **E:** Percentage Poaceae in pollen assemblages.

samples were analyzed at the Center of Geochronological Research (CPGeo), University of São Paulo (Brazil). Samples of 10 cm^3 of bulk sediment were freeze-dried and ground with an agate pestle and mortar. All chemical procedures were carried out in an ultra-clean laboratory class 10,000, equipped with a laminar flow fume hood class 100. For decarbonation, powdered samples were washed with ultra-pure water and reacted with a solution of hydrochloric acid, sodium acetate and ultra-pure water. The carbonate-free sediment powder was dissolved by acid digestion using HNO3 + HF + HCl (purified in the sub-boiling device Distiller STD-1000 at low temperatures) in discrete steps in teflon beakers (Savillex®), at a temperature of 100 °C. The Nd was separated from other rare earth elements first by a specific resin (RE-Spec) and second by the resin Ln-Spec. Then, Nd samples were deposited in rhenium parallel filaments with the addition of ultra-pure H_2O. The $^{143}Nd/^{144}Nd$ ratios were obtained by thermal ionization mass spectrometry (TIMS), using a Finnigan Triton mass spectrometer. Replicate analysis of JNdi standard (n = 19) yielded $^{143}Nd/^{144}Nd = 0.512093 \pm 0.000009$ (1σ). Nd procedure blanks were about 70 pg. The $^{143}Nd/^{144}Nd$ values were normalized to $^{146}Nd/^{144}Nd = 0.7219$ (DePaolo, 1981) and expressed in the ε_{Nd} notation, that is normalized by present-day chondritic uniform reservoir (CHUR) $^{143}Nd/^{144}Nd$ value, namely 0.512638 (Jacobsen and Wasserburg, 1980).

3.3. Palynology

In total, 154 palynological samples were taken at 20-cm intervals from the same sediment horizons as the foraminifera samples that were analyzed to establish the age model (Ferreira et al., 2021). Sample preparation was undertaken at the U.S. Geological Survey (Reston, Virginia, USA) following the methods of Faegri and Iversen (1975), Doher (1980), Traverse (1988) and Brown (2008). Sample size was approximately 10 g of dry sediment. Hydrochloric acid was used to remove all calcareous material, and cold hydrofluoric acid was used to dissolve silicate minerals. Processing continued by using acetolysis and potassium hydroxide (KOH). Due to the low pollen concentration in deep marine deposits, wet-sieving was performed using a150 μm mesh to remove larger particles and a 5 μm mesh to remove smaller ones and amorphous organic matter. In rare cases, pollen abundance was further enriched by heavy liquid separation using zinc chloride ($ZnCl_2$) with a density of 2.1 specific gravity. At least two slides per sample were prepared with glycerin jelly for investigation under the light microscope and the remaining material was stored in distilled water at the U.S. Geological Survey in Reston. One *Lycopodium clavatum* spore tablet (batch number 938934, average number of spore 10,679) was added at the beginning of the sample preparation to allow calculation of pollen concentrations (Stockmarr, 1971).

Identification of pollen and spores was based on comparison with several pollen atlases (e.g. Roubik and Moreno, 1991; Colinvaux et al., 1999; Silva et al., 2016), online databases (e.g. Bush and Weng, 2007), publications (e.g. Burn and Mayle, 2008; Gosling et al., 2009; Barros et al., 2013), and the tropical pollen reference collection of Frank E. Mayle (University of Reading, United Kingdom).

In samples with low pollen abundance, at least one slide was fully counted to enable the calculation of pollen concentration along the entire core. The pollen sum of 100 percent was calculated excluding fern spores and Poaceae due to an unusual high presence of grains in all samples. (Supplementary Table 2). Additional calculations for Poaceae abundance used the entire pollen count. Environmental interpretations are based on a subset of 79 palynological samples, in which more than 150 grains were counted and Poaceae pollen comprised less than 60%, providing a reliable vegetation description. Pollen data were summarized in a diagram in the software R (R Core Team, 2020) using the packages “Rioja” (Juggins, 2020) and “Vegan” (Oksanen et al., 2019). Pollen data were log-transformed and analyzed using Principal component analysis (PCA; Kenkel, 2006; Legendre and Birks, 2012) using PAST (Hammer et al., 2001). Various datasets containing all samples and taxa, as well as on the limited 79 sample dataset that excluded Poaceae (dominance) and Cyperaceae (because their thin wall impacted preservation in the deeper section of the core; Li et al., 2005; Jantz et al., 2013), were utilized to examine potential biases.

Pollen abundances were used to reconstruct biome affinity scores. Each pollen taxon was assigned to one or multiple plant functional types (PFTs) and each PFT was assigned to one or multiple biomes following Prentice et al. (1992, 1996) and the classifications of Marchant et al. (2009). This process of ‘biomisation’ represents a globally applied objective method (Izumi and Lézine, 2016; Tian et al., 2018; Altolaguirre et al., 2020) to use pollen data for biome reconstructions on the basis of standard algorithms taking into account that individual species distributions occur across various biomes and ecosystems. The applied classification uses 26 PFTs distinguished by the structure, leaf form, phenology, and climatic adaptions of plants (Prentice et al., 1996). In this context, a PFT represents a vegetation unit with an affinity relative to three environmental parameters: namely temperature, seasonal warmth and the Priestley-Taylor coefficient (α) of plant available moisture further explained in Marchant et al. (2009). A full description of the 26 PFTs can also be found in Marchant et al. (2009). Calculations used the software Biomise 3.0 developed by Ben Smith (University of Lund, Sweden) following the statistical background of Prentice et al. (1996). Results show the biome affinities of each sample, providing estimates of the most likely biome for each palynological assemblage. Newly assigned plant taxa followed Plants of the World Online (http://www.plantsoftheworldonline.org/), the IUCN red list of threatened species (http://www.plantsoftheworldonline.org/), Reflora (http://reflora.jbrj.gov.br/), eflora of Ecuador (http://www.efloras.org/flora_page.aspx?flora_id=21), GBiF (https://www.gbif.org/), BIEN (https://biendata.org/), Useful Tropical Plants (http://tropical.theferns.info/), the Gymnosperm Database (https://www.conifers.org/), and selected other publications (e.g. Reese and Liu, 2005; Gosling et al., 2009; Ortuño et al., 2011). All associations are summarized in Supplementary Table 3.

Biodiversity indices also were calculated based on pollen counts using PAST (Hammer et al., 2001) to increase the evaluation of taxonomic richness against taxonomic evenness (Pardoe et al., 2021). A combination of biodiversity metrics was used to overcome the shortcomings of single parameter methods; selected metrics included the Shannon heterogeneity index (Shannon H Index) to determine the diversity of assemblages and address the issue of varying pollen counts per sample, taxonomic evenness to compare the relative abundance of pollen taxa in different assemblages, dominance to highlight if single taxa comprise the main count of a sample, and rarefaction analysis set to a sample size of 100 counted pollen grains to standardize diversity measurements among the different samples (Pardoe et al., 2021 and references therein). The full range of reconstructed biodiversity metrics is summarized in Supplementary Table 4.

4. Results

4.1. Sedimentation rates and ε_{Nd}

CDH-79 recorded sedimentation rates (Ferreira et al., 2021) of 1.52 cm/kyr between 1930 and 400 ka and 6.69 cm/kyr during the last 400 ka (Fig. 3B). Peak rates, exceeding 10 cm/kyr, occurred only

in the time interval from 400 ka to the top of the core. An event at 26.44 to 26.35 ka had an exceptional accumulation rate of ~110 cm/kyr (Supplementary Table 1).

The ε_{Nd} ratios vary only slightly, ranging between −12.10 and −14.17 with an average of −12.91 (Fig. 3C). The Andean-dominance in the terrestrial provenance remains the consistence source of terrestrial material of the CDH-79 record showing no indication of stronger river-inflow from e.g. the Northeast. Therefore, the Amazon draingage basin is the source of the terrestrial sediment throughout the entire 1800 ka record at site CDH-79 (Supplementary Table 1).

4.2. Palynology

4.2.1. Pollen abundances

Pollen concentrations in CDH-79 are low during the entire study interval, ranging from zero to 1971 pollen grains/g of dry sediment (Fig. 3D; Supplementary Table 2). All samples below 3104 cm core depth are barren, limiting the basal age of the pollen record to 1796 ka. Pollen concentrations in the uppermost section, covering the last 218 ka, exceed 100 grains/g and the highest concentrations >1000 grains/g occur in the samples deposited between 1354 and 1203 ka. Pollen and spore concentrations display similar trends, with higher values between 1600–1500 ka and 800–600 ka due to higher spore occurrences (Supplementary Fig. 1; Supplementary Table 2). In general, higher pollen concentrations were found in interglacial sediments (Fig. 3D). Fern spores reached values exceeding 80% relative to all pollen and spore counts with an average of 63% (Supplementary Fig. 1). Identified fern spore taxa primarily include genera of the Polypodiaceae family followed by genera from the Cytheaceae and Selaginellaceae families. The abundances of all ferns displayed little variation with core depth (Supplementary Table 2).

Poaceae is the most abundant pollen taxon found in CDH-79, which showed a significant, somewhat step-wise, decrease from the base towards the top of the core (Fig. 3E; 4). Average values of 60% in older samples decreased after 1300 ka to levels around 50%. These values persisted until approximately 700 ka, when the abundance again decreased to about 40% in the entire remaining portion of the record. PCA (supplementary material) supports a major shift in the pollen assemblages between 900 and 700 ka considering all samples and all pollen taxa.

Changes around ~758 ka are evident using the limited pollen record (subset of 79 samples, see Material and methods), which holds similar results in both analyses considering the entire log-transformed pollen dataset and excluding Poaceae (due to its overrepresentation) and Cyperaceae (apparent preservation bias). CONISS analysis indicates important vegetation changes around ~960 ka, 758 ka and 300 ka (Fig. 4). In the core section older than 758 ka, *Alchornea*, *Hedyosmum*, and *Borreria* dominats the pollen spectrum, while the younger section is characterized especially by Arecaeae, Moraceae-Urticaceae, and *Piper* (supplementary material). Additional important elements contributing to the pollen spectra are Asteraceae, Rubiaceae and Solanaceae, which increased from the base until ~500 ka and remained high thereafter, opposed by decreasing trends in *Alchornea*, Apiaceae, and Melastomataceae-Combretaceae (supplementary material). Additional important components in the pollen record including *Mauritia*, Bignoniaceae, Apocynaceae and Araceae exhibited no clear trends in the entire record (Fig. 4; Supplementary Table 2).

4.2.2. Biome reconstruction

Seventy-nine samples were included in the biome reconstructions (Fig. 5; Supplementary Table 3). The majority of samples indicated warm temperate rainforest (WTRF) as the most likely biome on the basis of the pollen assemblage with several

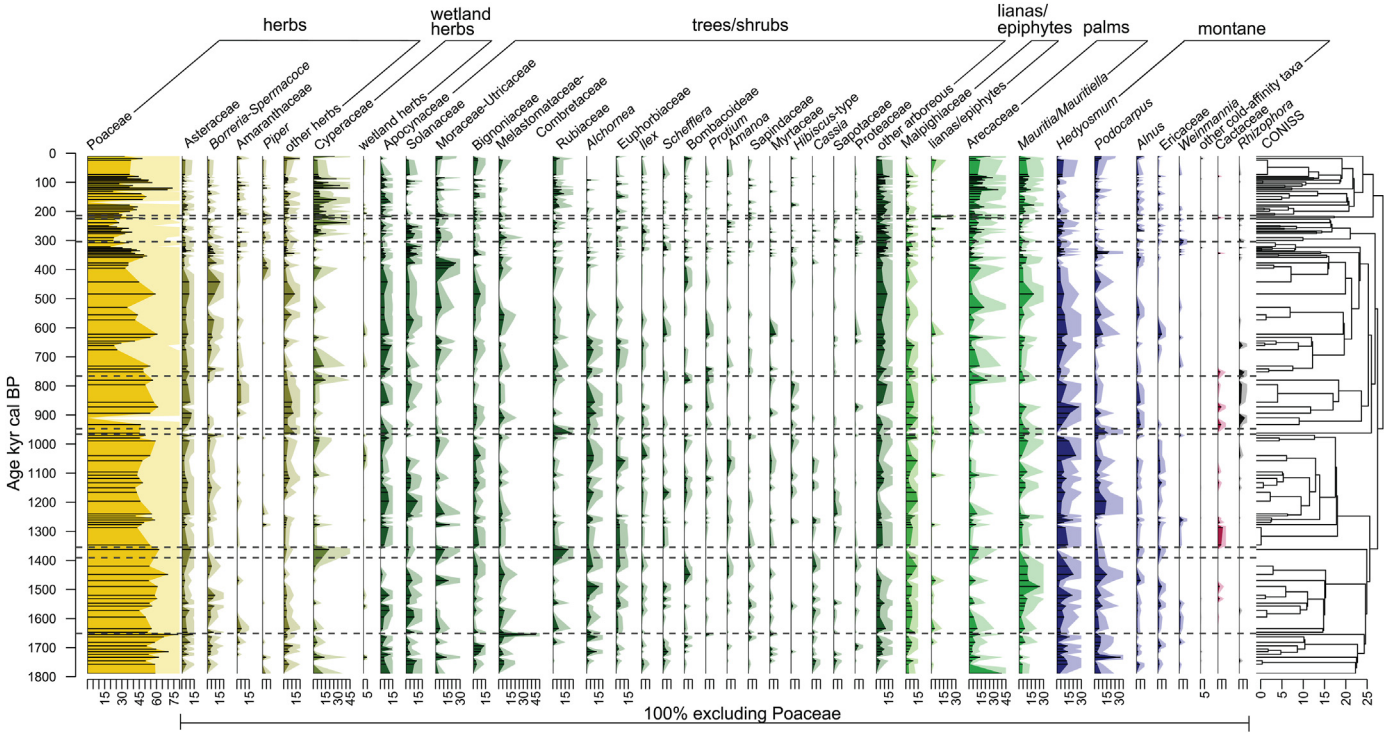

Fig. 4. Pollen diagram of the marine sediment core CDH79. Samples with pollen counts higher than 50 were included in the diagram resulting in 120 samples. CONISS analyses were based on log (x+1)-transformed relative abundances of pollen taxa. Poaceae were excluded from the 100% pollen sum and CONISS calculation while Poaceae abundance was calculated by using the total pollen sum.

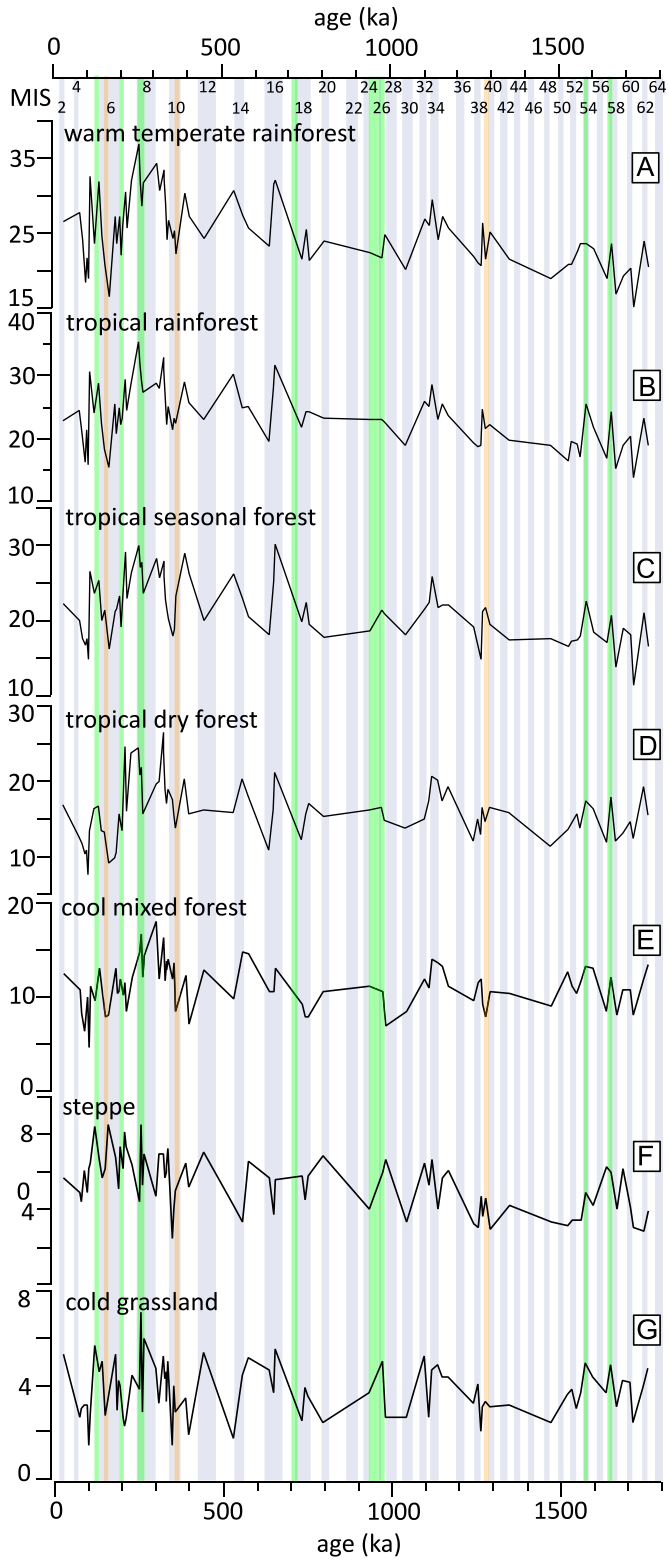

Fig. 5. Reconstructed biome affinity scores calculated following the associations of Marchant et al. (2009) for the reduced sample set of 79 samples covering the last 1800 ka; grey vertical bars mark glacial stages. Marine Isotope Stages (MIS) are numbered in the top of the figure. Green bars indicate samples of tropical rainforest (TRFO; Table 1) dominance while orange bars highlight the samples with a dominance of tropical seasonal forest (TSFO; Table 1). (For interpretation of the references to colour in this figure legend, the reader is referred to the Web version of this article.)

exceptions: tropical rainforest biome (TRFO) was dominant in ten samples (1653, 1579, 985, 939, 758, 738, 264, 260, 201, 122 ka); three other samples revealed highest biome scores for the tropical seasonal forest (TSFO) (1283, 365, 155 ka) (Fig. 5; Supplementary Table 3). The long-term trend of many biomes through time showed general similarities due to the shared taxa and PFTs indicated by positive correlation factors (Supplementary Table 3). Strong correlation occurred between the lowland rainforest biomes (TRFO; TSFO) and the WTRF with values above 0.9 (Pearson linear correlation) due to a generally increasing trend throughout the record (Fig. 5A, B and C; Fig. 6A).

A trend towards higher amplitude oscillations in forested biomes up-core is visible after ~750 ka, and even more notably in the last ~400 ka (Fig. 5A–D). The higher elevation forest biomes of the cold temperate rainforest (CTRF) and cold mixed rainforest (COMI; Fig. 5E) correlated with 0.88 and shared high similarities with the lower elevation warm mixed forest (WAMF) and the warm temperate evergreen forest (WEFO) (Fig. 6A). The desert (DESE) and steppe (STEP) biomes show the lowest correlation with all other biomes (below 0.35) (Supplementary Table 3; Fig. 6A). STEP (Fig. 5F), DESE, and the high elevation cool grassland (CGSS) and cool grass- and shrubland (CGSH, Fig. 5G) have strong fluctuations in their affinity scores, yet do not show clear trends through time (Supplementary Table 3). PCA further reveals a shift in statistical distances between the biomes following the division suggested by CONISS at 758 ka (Fig. 4). In the sequence between 1800 and 758 ka, mainly the higher elevation biomes (COMI; CTRF; CGSH; CGSS) show a clear distinction (Fig. 6B). In contrast, in the section younger than 758 ka, the lower elevation dense forests (TRFO, TSFO) and the low elevation forests (WTRF) form a clear group with higher distance from the TDFO (Fig. 6C).

4.2.3. Biodiversity metrics

The highest pollen concentrations occurred in the intervals between 1400 and 1100 ka and between 350 and 100 ka (Fig. 7A). These intervals also have the highest diversity of pollen taxa with a maximum number of 68 identified pollen taxa per sample at 201 ka (Supplementary Table 4). Between 1800 and 1500 ka, results show high dominance and low evenness values (Fig. 7B; C). While dominance decreased more or less continuously through time without strong variations, the evenness of the pollen assemblages remained low until reaching a peak around 700 ka, with higher values during the last 300 ka. This is a similar trend to that expressed by rarefaction (T100) and Shannon H Index, which are highest between 342 and 196 ka (Fig. 7D) indicating an interval of high biodiversity (Fig. 7E). Biodiversity also was slightly higher during the earlier interval of high pollen concentration and numbers of taxa numbers, between 1300 and 1100 ka. All reconstructed biodiversity indices are summarized in the Supplementary Table 4.

5. Discussion

5.1. Depositional setting and taphonomy

The ε_{Nd} values range only slightly between −12.10 and −14.17 (Fig. 3C) indicating that the terrestrial sediment arriving at core site CDH-79 was continuously composed of an Amazon River source during the last 1800 ka. These ε_{Nd} isotopic values are similar to other marine deposits with Amazon provenance (e.g., Zhang et al., 2015; van Soelen et al., 2017; Hoorn et al., 2017). These values further point to the dominance of Andean-derived sediments among the Amazon detritus (e.g., Höppner et al., 2018) and contrast with other known tropical South American rivers transporting sediments from cratonic sources (Guiana and Brazilian Shields),

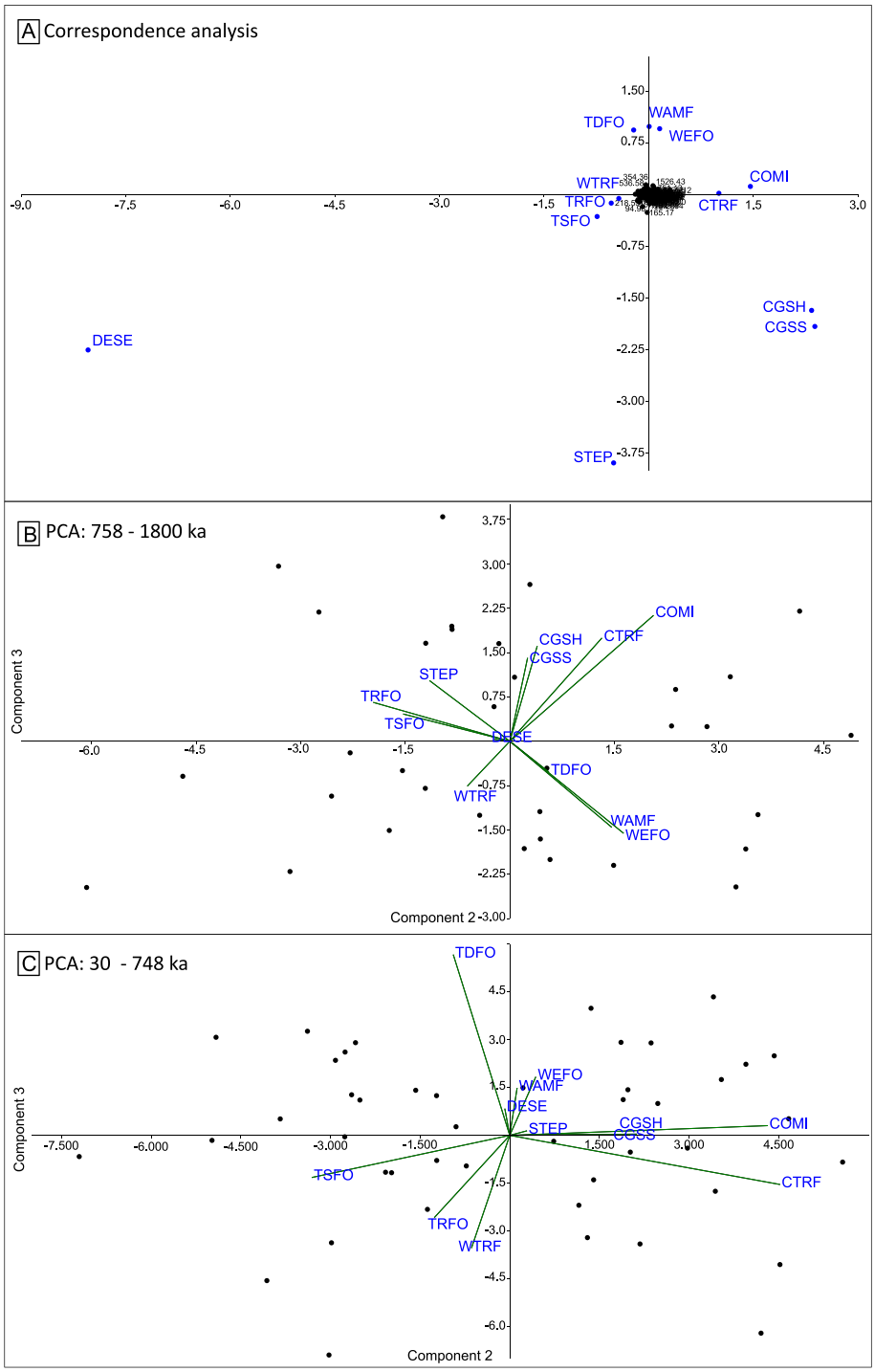

Fig. 6. Statistical analysis of the biome affinity scores; A: Correspondence analysis of all the biome affinity scores (all samples); B: Principal component analysis (PCA) of all samples between 1800 and 758 ka; C: Principal component analysis (PCA) of all samples between 748 and 30 ka. Biome abbreviations follow the description in Table 1 and Supplementary Table 3.

which all have values less than −16. Less radiogenic ε_{Nd} signals are also reported for marine sediments off NE Brazil that derived sediment from rivers draining the Brazilian Shield (e.g. Zhang et al., 2015; Sousa et al., 2021).

Cratonic rivers, such as the eastern Amazonian tributaries, must also constitute at least minor amounts of the sediment in CDH-79 hence contribute to the ε_{Nd} isotopic signal of core CDH-79 in addition to the dominant sediment input from the Andes (Meade, 1994). An increase in river runoff from eastern Amazonia relative to the Andean-sourced rivers that contribute to western Amazonian tributaries, would produce small shifts in ε_{Nd} towards less radiogenic values (Figs. 1A and 3C). Variations in precipitation distribution between eastern and western Amazonia have been previously postulated for Heinrich stadials and glacial stages, resulting in slight changes in the composition of Amazonian sediments delivered to the ocean (Höppner et al., 2018; Crivellari et al.,

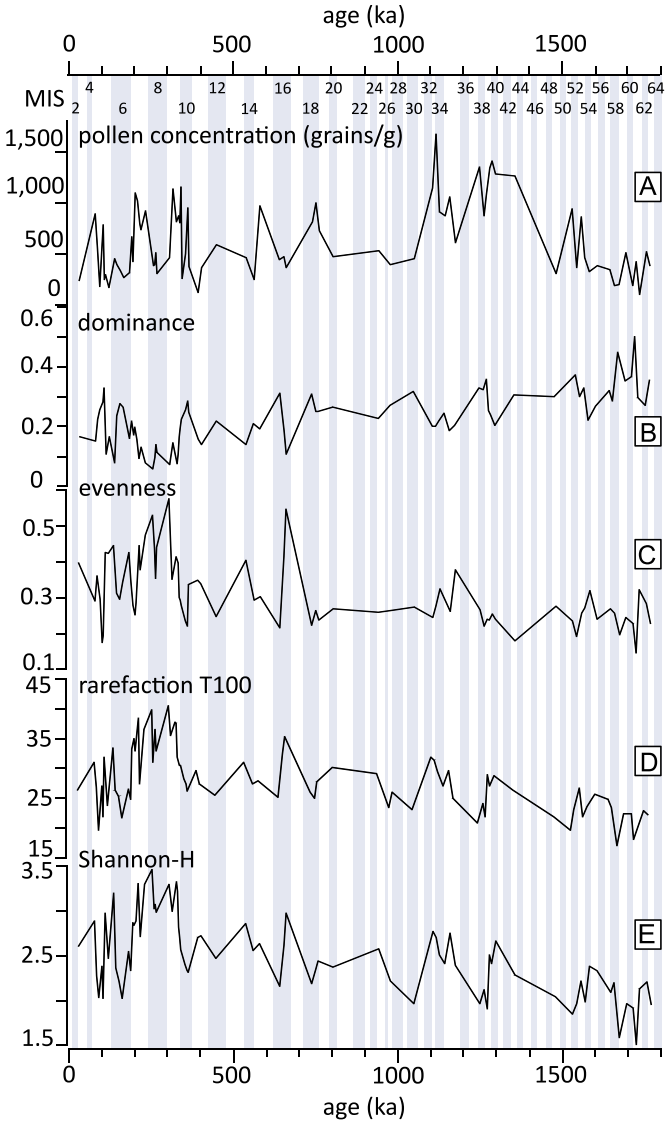

Fig. 7. Selected biodiversity metrics of the reduced sample set of 79 samples from CDH-79 showing A: pollen concentration (pollen per gram dry sediment); B: Dominance (Simpson Index); C: Evenness (homogeneity of each pollen sample considering the total counts); D: Rarefaction T (100) (re-calculated biodiversity to a standard pollen count of 100); E: Shannon H Index (indicator that considers pollen counts per sample and dominance of pollen types). Vertical grey bars indicate glacial stages; marine Isotope Stages (MIS) are numbered in the top of the figure.

2019; Mason et al., 2020). Lower global mean sea level (Fig. 2; 3) did not significantly alter the transport of terrestrial material to the seamont (Abe-Ouchi et al., 2015). A predominantly Amazon River provenance for the sediments deposited at site CDH-79 is further supported by the observations of pollen of plants with current distributions limited to the Andes. Most significantly, this includes *Alnus* (Fig. 4), but also rarer occurrence of other Andean-limited taxa, specifically *Polylepis*, *Ephedra* and *Balbesia,* are found throughout the entire record (Supplementary Table 2).

Although the location of the CDH-79 is southeast of the Pleistocene Amazon Fan, our data indicate a constant input of terrestrial material from the Amazon River to the top of the seamount (Fig. 1; 2). As modern surface circulation in this region is dominated by the NBC (Fig. 2A), which carries Amazonian suspended sediment to the northwest (Govin et al., 2014; Zhang et al., 2015; Häggi et al., 2017), another mechanism must be responsible for the delivery of Amazonian sediment to the CDH-79 site. While the bulk fraction is carried to the northwest by the NBC, part of the Amazonian terrigenous sediment is transported southeastward (Damuth et al., 1995; Häggi et al., 2016; Höppner et al., 2018) by the southward flowing DWBC (Fig. 2B). Presumably, sediments settling from the DWBC accumulated slowly atop the seamount, consistent with the low sedimentation rate of the CDH-79 record (Fig. 3B).

Bulk sediment accumulation rates at site CDH-79 show higher values after 400 ka (Fig. 3B), co-occurring with a significant increase in pollen concentration since Marine Isotope Stage (MIS) 10 (359 ka; Fig. 3D). During this time period, we observe accumulation rates and pollen concentrations were greater during interglacial stages than glacial stages. This visual observation at CDH-79 contrasts with previously published deep marine sedimentary records from the continental slope and Ceara Rise which generally indicate increased Amazonian sediment mainly controlled by decreased sea-levels (Flood and Piper, 1997; Curry and Cullen, 1997; Harris and Mix, 1999; Mason et al., 2020). Possibly, higher velocity of the DWBC during interglacial stages relative to glacial stages (Poirier and Billups, 2014; Howe et al., 2016) favored this deep southeastwards transport of Amazonian sediments towards seamount site CDH-79.

5.2. Vegetation and biome reconstruction

5.2.1. Vegetation history of the Amazonian drainage basin

The pollen assemblages recorded in CDH-79 were the result of a long and complex transport across the Amazon drainage system and the western equatorial Atlantic (Fig. 1; 2), that was variably impacted by changes in precipitation, and river hydrology on the continents (Jennerjahn et al., 2004; Musher et al., 2022), as well as offshore variations in sea level and the strength and position of ocean currents (González and Lupont, 2009; Piacsek et al., 2021). The impact of these collective taphonomic factors is impossible to quantify in this record.

Increases in pollen concentration and biome affinity scores (Fig. 3; 5) appear to co-vary, although low statistical correlation among these proxies (between 0.12 and −0.11; Supplementary Table 4) suggest that independent mechanisms determined pollen transport. Due to the low correlation between pollen input and its content (Supplementary Table 4) and the constant presence of typical elements of Amazonian sourced pollen assemblages (e.g. *Alnus, Hedyosmum, Podocarpus, Alchornea,* and others) (Haberle, 1997; Hoorn, 1997; Hoorn et al., 2017), the changes in the pollen record mainly represent shifts in the vegetation within the Amazon drainage basin. Nevertheless, taphonomic factors may also play a role, although are yet to be investigated.

In our biome reconstruction, biomes are treated as physiognomic units representing the vegetation within the Amazon drainage basin (Prentice et al., 1992; Marchant et al., 2009). The highest biomes scores during the last 1800 ka indicated a dominance of warm temperate rainforest (WTRF), followed by the tropical rainforest (TRFO) (Fig. 5A; B; Table 1). These high values of the WTRF biome scores could result from a combination of three different mechanisms: (1) a significant expansion of low-elevation elements into the lowlands; (2) a constant mixture of pollen from different elevations in the pollen assemblages; (3) a statistical artifact due to the high number of taxa shared with the TRFO (Marchant et al., 2009; Supplementary Table 3). After critically evaluating each mechanism, a combination of (2) and (3) is considered most likely. Marine sediment deposits produced by Amazon River discharge constantly receive pollen from the entire drainage basin, consistent with the observed mix of elements from vegetation types of low and high elevations. Moreover, many plants today have an overlapping distribution between the TRFO and

WTRF which is expressed in shared PFTs constructing the biome scores (Supplementary Table 3). The integration of pollen gathered across the basin during transport and the shared plants of both rainforest types probably resulted in the highest scores for the WTRF. This does not necessarily indicate the dominance of low-elevation elements in the Amazonian lowlands, but rather supports the conclusion that the Amazon Basin remained mostly forested over the entire Pleistocene with biotic turnover associated with glacial-interglacial cycles (Fig. 5). However, there is evidence that cold-affinity taxa did increase in lower elevations and possibly in lowland forests during the glacial stages (e.g. Colinvaux et al., 1996; Fontes et al., 2017; Reis et al., 2022).

Despite the low temporal resolution of our reconstruction, the affinity scores of the TRFO and WTRF show an increase over the last 1800 ka. This was caused either by an expansion of lowland and low-elevation rainforests, a higher input of pollen from these vegetation units potentially caused by increased runoff from tropical rainforest areas, a progressive decrease of floodplains and higher contribution of uplands or a combination of those factors. Both rainforest types (TRFO and WTRF) are positively correlated with all biodiversity indices (Fig. 7D; E), especially the rarefaction (both >0.85) and Shannon H Index (TRFO 0.76; WTRF 0.79). A negative correlation between the TRFO and the WTRF and the dominance index (TRFO -0.73; WTRF -0.77) is also observed, indicating the high diversity (Giesecke et al., 2014; Pardoe et al., 2021), particularly during the last 400 ka. No additional biome scores are significantly correlated with biodiversity metrics (Supplementary Table 4). This confirms the prevalence of these rainforest types relative to other biomes within the Amazonian drainage basin through the entire record and suggests the diversity of the lowland rainforests may have increased through time. Another possibility is that the progressive decrease of Poaceae over the last 1800 ka may suggest a retraction of floodplains while the contribution from more diverse uplands increases.

Between 1800 ka and 1500 ka, ongoing long-term Pleistocene cooling had an impact on the cold-adapted vegetation in the Andes while lowland units appeared stable. Therefore, the high elevation vegetation is the only clearly distinct group in the lower section of CDH-79 (Fig. 6B). Signals of the expansion of high elevation vegetation coincided with high peaks of *Podocarpus*, *Hedyosmum* and *Alnus* (Figs. 4 and 5E; G), whereas tropical rainforests might have been dominated by few taxa as indicated by lower biodiversity indices (Fig. 7D; E). Between 1400 and 1100 ka high peaks in pollen concentration occurred and biodiversity metrics began a progressive increase associated with an expansion of TRFO and WTRF peaking towards MIS 33 and MIS 31. At 1100 ka, an opposite trend set in, with comparable decrease in lowland and montane forests. During this period (1000–800 ka), herbaceous taxa such as *Borreria*, Asteraceae, *Gomphrena* and *Alternanthera* suggest an increase in open (STEP and DESE) and seasonal vegetation (TDRF) pointing to a significant expansion of a distinct dry season in at least parts of the Amazonian drainage basin (Fig. 4; 5; Table 1). While the herbaceous-dominated biomes of the high Andes (CGSH and CGSS) were continuously represented between 800 and 600 ka (Fig. 5G), cold forest biomes remained stable during this time interval, resulting in low biodiversity signals, high dominance and low evenness (Fig. 7).

While interpretation of the stability of vegetation is inconclusive due to the low temporal resolution and low pollen concentration between 800 and 400 ka, a distinct new dynamic in Amazonian vegetation began around 400 ka. This is marked by increased pollen concentrations and accumulation rates and a major expansion of TRFO and WTRF and of biodiversity indices (Fig. 3; 5; 7). During warm MIS 9 and 7, the TRFO dominated, whereas during cooler MIS 10 and MIS 6, seasonal forests (TSFO) were the major biome in the Amazon drainage basin in some individual samples (Fig. 5; Supplementary Table 3). This suggests a higher water stress on plants but not a significant opening of the canopy. The hypothesis of extensive open savanna within the Amazonian lowlands dates back to Haffer (1969), who posited that the separation of rainforest refugia by open grasslands during past glacial stages was an important mechanism for producing the high biodiversity of the Amazonian lowlands. An expansion of savanna has been reconstructed based on vegetation models (Allen et al., 2020; Sato et al., 2021) and is supported by pollen studies at the margins of the Amazon rainforest (Hermanowski et al., 2012; Fontes et al., 2017; Reis et al., 2017). However, interpretations of savanna expansion have focused on Poaceae as a key ecological indicator for grasslands (Maksic et al., 2022). Yet, despite numerous uncertainties in the interpretation of the CDH-79 record and its relative low temporal resolution, there is no clear signal for an expansion of TDRF or STEP and likewise there is no evidence for any substantive expansion of open savanna vegetation in favor of the TRFO during any glacial interval (Fig. 5D, F). Results of LGM model experiments, under atmospheric CO_2 concentrations of 180 ppm and 4 °C lower-than-pre-Industrial temperature (Beerling and Mayle, 2006; Maksic et al., 2022) suggested that western and central Amazonian evergreen tropical rainforest persisted during glacial stages in agreement with the biome reconstruction. In addition, these models showed eastern Amazonia may have experienced drier conditions and increased patches of tropical seasonal forest or deciduous broadleaf forests as well as reduced tropical rainforest at the margins of Amazonia. Our data support such a scenario for previous glacial stages during the last 400 ka, where fragmentation of the rainforest may have occurred seasonally and separation by open vegetation was limited. Pollen indicators of open grasslands other than Poaceae, such as *Gomphrena* and *Alternanthera*, occurred in both glacials and interglacials, although their climatic significance may be somewhat obscured due to the large and climatically-heterogeneous catchment system of the Amazon River and its tributaries (Fig. 1; 4). Considering the higher proportion of Amazonian lowland pollen input from eastern Amazonia to the Atlantic (Akabane et al., 2020), the CDH-79 pollen data presumably also reflect the tropical seasonal forest primarily present in eastern Amazonia during MIS 10 and MIS 6. During MIS 8, TSFO also increased but values did not exceed those of the tropical low elevation and lowland rainforest (Supplementary Table 3). Yet, higher abundance of the steppe vegetation during MIS 8 and 6 further points to a relative glacial expansion of semi-arid vegetation, although some peaks are also recorded during interglacial stages. It may be that the expansion of savanna did not occur exclusively during glacial stages or might have occurred in different times in the northern and southern part of the Amazonian drainage basin (Bueno et al., 2017). Nevertheless, the CDH-79 record shows continuous rainforest vegetation in glacial stages prior to the LGM, supporting the hypothesis of a seasonally fragmented, but densely forested, vegetation cover.

During glacial stages of the last 400 ka, high elevation Andean biomes reached their highest values (Fig. 5E; G; Supplementary Table 3). A presumed xpansion of all cold biomes occurred almost simultaneously during cooler temperatures in glacial periods with highest affinities of the entire record during MIS 12 and 8. Glacial values of COMI and CTRF are strongly controlled by the abundance of *Alnus*, while the herb *Borreria* also increased significantly during MIS 12, 10 and 8 (Fig. 4). Characteristic cold-adapted elements, such as *Hedyosmum* and *Podocarpus*, contribute less to the cold biome reconstruction during the last 400 ka despite their importance in many LGM records (e.g. Colinvaux et al., 1996; Lima et al., 2018).

5.2.2. Poaceae in the CDH-79 record

CDH-79 recorded unusually high levels of Poaceae (30–65%) in comparison with the modern Amazon River (<20% in Haberle, 1997; <30% in Akabane et al., 2020) and previous marine palynological studies (<20% in Haberle, 1997; <40% in Hoorn et al., 2017). Although strong signals of grasses were previously interpreted as an expansion of grassland in the lowlands or high Andes (e.g. Hermanowski et al., 2012; Hoorn et al., 2017; Fontes et al., 2017), our data often show opposing trends between Poaceae and savanna and grassland vegetation types (STEP, TDFO; Fig. 5). In this biome analysis, Poaceae is not assigned to any of the applied biomes (Marchant et al., 2009) because of its wide ecological distribution (e.g. Bush, 2002; Marchant et al., 2009; da Silva et al., 2020; Akabane et al., 2020). As a consequence, biome calculations are based on more ecologically distinctive taxa, none of which support the presence of expansive savanna grasslands (TDFO or STEP) or more widely distributed montane grasslands (CGSS or CGSH) over the last 1800 kyr (Fig. 5D; F). Although the total number of grass pollen grains certainly represents a mixture from various biomes, we consider the abundance of Poaceae was from a proximal source, such as azonal vegetation along the rivers and the coast. Previous studies of modern Amazonian sediments showed the highest concentrations of grass pollen in the Amazon estuary as well as the Pará River and the Tapajós-Amazon confluence (Akabane et al., 2020), and the highest values of grass pollen were found in suspended sediment east of Santarem (Haberle, 1997). In these areas, herbaceous plants dominate the modern riparian wetland vegetation (Melack and Hess, 2011; Hess et al., 2015) and Poaceae is both common and a prolific pollen producer. Combing the herbaceous wetland indicator taxa determined by Akabane et al. (2020) (excluding Cyperaceae due to its strong preservation bias) and *Alchornea* as a riparian component (Burn et al., 2010), the data shows a consistent pattern with the abundance of Poaceae in CDH-79 (Fig. Supplementary Fig. 2; Supplementary Table 2). In addition, palynological analysis of Cenozoic sediments from Amazonian riverbanks commonly exhibit Poaceae as the main taxa, likely associated with wetlands deposits (swamps, floodplains) (e.g. Latrubesse et al., 2010; Pupim et al., 2019).

In CDH-79, Poaceae reached the highest abundances before 1300 ka, but favorable conditions continued until 700 ka (Fig. 3E; 8 F). At this time, all wetland indicators declined coinciding with the transition to higher amplitude sea-level oscillations (Fig. 8G), which may have played a significant role in shaping the long-term fluvial system (Irion et al., 2010). Subsequently, low values of Poaceae and wetland elements co-occurred with an overall vegetation transition between 800 and 600 ka (Fig. 4; supplementary material), when biodiversity metrics began a progressive increase associated with an expansion of TRFO and WTRF (Fig. 8C; D). Furthermore, there is no clear correlation between Poaceae and climatic variations, as peaks in abundance occurred during both glacials and interglacials (Fig. 8F).

5.2.3. Appearance of Alnus in South America

Alnus is present in CDH-79 throughout the entire 1800 kyr record. It appears in all pollen-containing samples and reaches a maximum value of 5.4% (Fig. 4; Supplementary Table 2). The modern distribution of *Alnus* in South America is limited to the Andes, where it occurs in the montane cloud forest zone (COMI; CTRO; Marchant et al., 2009). In certain areas where the cloud forest is more open, *Alnus* forms monospecific stands (Brown et al., 2001), and it also successfully colonizes disturbed areas as a pioneer taxon due to its rapid growth (Blodgett, 1998; Wicaksono et al., 2017). Pollen grains of *Alnus* are commonly found in modern Amazon River samples (Haberle, 1997; Akabane et al., 2020) as well as in Pleistocene marine deposits receiving Amazon River

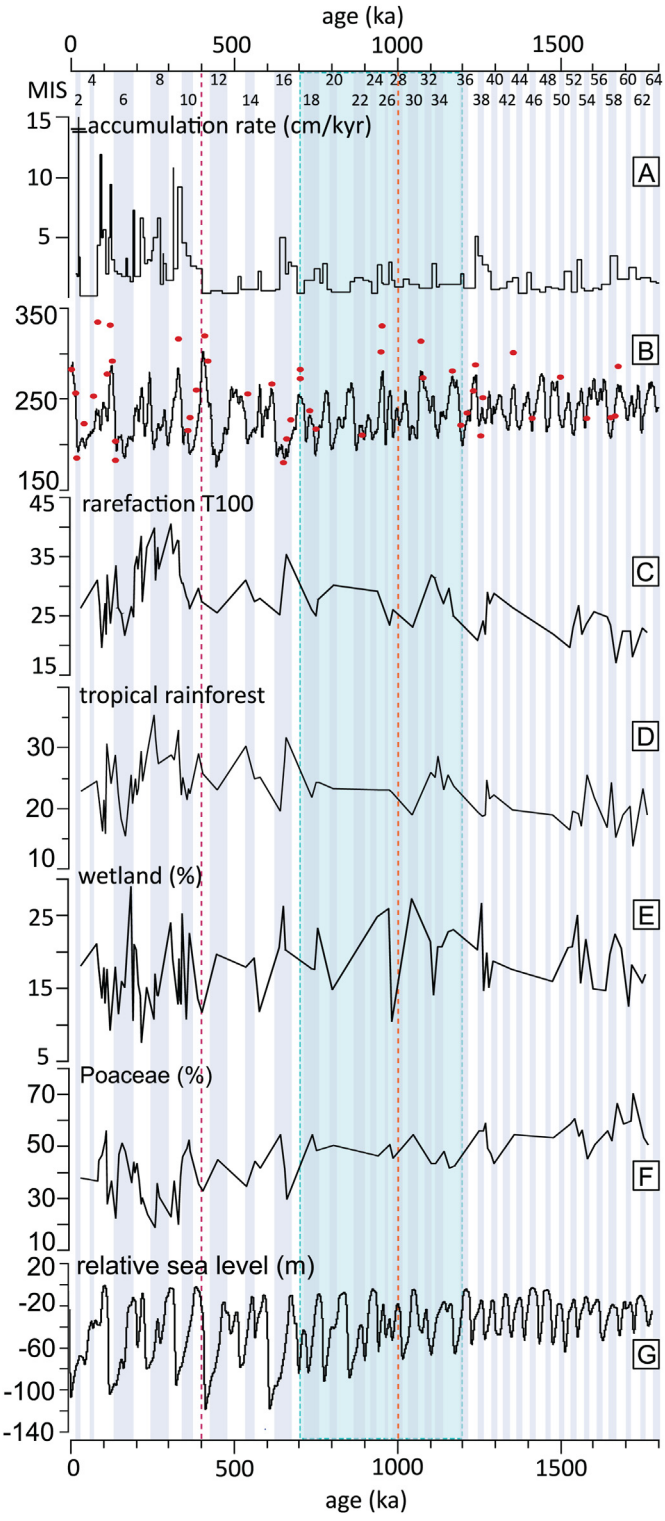

Fig. 8. Comparison of various proxies of the last 1800 ka to data from CDH-79. A: CDH-79 accumulation rate; B: reconstructed values of atmospheric CO_2 (red dots) are based on boron isotopes (Hönisch et al., 2009) and compared with the modelled CO_2 levels of Berends et al. (2021); C: T100 rarefaction represents biodiversity of CDH-79; D: biome affinity scores for the tropical rainforest; E: Percentages for wetland vegetation of total pollen counts (excluding Poaceae and Cyperceae; Supplementary Table 2); F: Poaceae percentages considering all pollen counts; G: modelled global eustatic relative sea level (de Boer et al., 2014). Vertical grey bars indicate glacial stages, and the turquoise panel represents the Mid-Pleistocene Transition (MPT); the orange dashed lines separates the early from the late MPT, while the dark red dashed line marks the onset of the last 400 ka following the Mid-Brunhes Event. (For interpretation of the references to colour in this figure legend, the reader is referred to the Web version of this article.)

runoff (e.g. Hoorn, 1997; Haberle, 1997; Piacsek et al., 2021). In general, during glacial stages, higher amounts of *Alnus* pollen are found in terrestrial pollen records of the western Amazon, possibly as a result of the downslope migration of *Alnus* into the Amazonian lowlands (Cohen et al., 2014; Lima et al., 2018). In CDH-79, *Alnus* pollen reached its highest values during MIS 10 and MIS 8 with a subsequent decrease in younger sediments (Fig. 4; Supplementary Table 2). High values (>5%) were also present at ~1500 and ~950 ka, indicating that *Alnus* was present in the parts of the Andes and that Andean pollen grains were consistently transported to the Atlantic Ocean by the Amazon River and its tributaries. *Alnus* abundances near or below 5% are comparable to values previously observed in late Pleistocene sediments of the Amazon Fan (Haberle, 1997; Hoorn, 1997), although these values were surpassed by peak values of 8% in the late Pleistocene and Holocene sediments from a marine core collected on the continental slope slightly southeast of core CDH-79 (Piacsek et al., 2021). The consistent occurrence of *Alnus* combined with the high number of up to 10 pollen grains per sample in the CDH-79 record (Fig. 4), strongly supports our interpretation that it reached the Amazon Basin in the earliest Pleistocene, agreeing with extra-Amazonian records from northernmost South American records (e.g. Germeraad et al., 1968; Pocknall et al., 2001).

The presence of Alnus as early as 1.8 Ma at CDH-79 stands in contrast to its first well-dated occurrence at 1 Ma in the Bogotá Basin of Colombia at an elevation of 2550 m (Hooghiemstra and Cleef, 1995; van der Hammen and Hooghiemstra, 2000; Torres et al., 2013). Previous studies indicate that *Alnus* migrated from North America to southern Mexico during cooling climates of the Pliocene (Graham, 1976, 1999), but other records in Central America remain unconfirmed (e.g. Neogene of Panama; Graham, 1999). In a previous pollen study of marine sediments from offshore Venezuela (Germeraad et al., 1968) noted the consistent presence of *Alnus* from the Paria Formation during Pleistocene. An early Pleistocene age of the Paria Formation was also provided by Macsotay (2005), which would support the hypothesis of an earlier arrival of *Alnus* in South America than previously estimated. Although no precise age is currently confirmed in the studies from Venezuela, the well dated sedimentary sequence of core CDH-79 clearly suggests an arrival of *Alnus* in South America prior to 1800 ka.

A later first appearance of *Alnus* in the Bogotá Basin in Colombia relative to the Amazon and Orinoco drainage basins is puzzling. *Alnus* in South America is associated with moist climates and high atmospheric humidity (Fournier, 2002; Weng et al., 2004). Similarly, European studies have documented delayed expansion of *Alnus* in arid regions (Douda et al., 2014). Prior to the first occurrence of *Alnus* in the Bogotá Basin at MIS stage 29 (1.01 Ma) in the Colombian records, the area was covered with a drainage system, lakes and swamps, where *Myrica* grew within the same niche occupied by *Alnus* today. A plain forest was present at higher grounds (Torres et al., 2013). After Myrica decrease significantly between 1500 and 1200 ka, *Alnus* was established in the vegetation of the Bogotá Basin; these changes have been correlated with large fluctuations in temperature and local tree line (Hooghiemstra and Ran, 1994; Hooghiemstra and Flantua, 2019). It is possible that the difference in first occurrences of *Alnus* among the sites reflect different migration routes related to variation in moisture availability, but further research is required to resolve this question.

5.3. Amazonian vegetation and global climate

Continuous dominance of rainforest vegetation across the lowlands that interchanges with warm temperate rainforests suggests the persistence of rainforest vegetation in the Amazonian drainage basin during the last 1800 kyr. Biome expansions and contractions were not necessarily coupled with glacial-interglacial cycles before 400 ka, although this pattern may be a product of the lower amplitude of climate variation prior to the Mid-Bruhnes Event (~430 ka; MBE; Barth et al., 2018) and is challenged by the low temporal resolution of this study.

The CDH-79 record indicates that the first significant expansion of lowland rainforests and of biodiversity occurred between 1200 and 1100 ka during the extremely warm interglacials of MIS 33 and MIS 31, which were separated by an unusually short glacial stage (Teitler et al., 2015; de Wet et al., 2016). Boron isotopes also hint at somewhat higher CO_2 levels during this time (Hönisch et al., 2009, Fig. 8B), which may have favored the spread of diverse tropical rainforest in Amazonia (Fig. 8C; D). Although higher CO_2 values during this time are not confirmed by model reconstructions (e.g. Willeit et al., 2019; Berends et al., 2021, Fig. 8B), global vegetation studies indicate favorable conditions that led to warmer and/or less seasonal vegetation (Tzedakis et al., 2006; Tarasov et al., 2013; Oliveira et al., 2017).

On the high Colombian Bogotá Plateau at 2550 m elevation, palynological records indicate that cool climatic conditions persisted during MIS 33 and 31, although alternatively the coincident upward migration of the sub-Andean forest line could imply a regional shift toward warmer conditions (Hooghiemstra, 1984; Torres et al., 2013). Following this apparently anomalous period, changes in the high Andean vegetation of the Bogotá Plateau resembled changes observed in CDH-79, which both record strong glacial pulses between 1000 and 850 ka. Lowland Amazonian vegetation reconstructions suggest cooler and presumably drier conditions during this time, resulting in a reduction of all types of forested vegetation (Fig. 5; 5) while modelled global CO_2 declined (Fig. 8B). This relatively cool and dry phase in the Amazonian realm coincides with the late MPT, global climate change related to substantial growth of the large Northern Hemisphere ice sheets (Chalk et al., 2017; Willeit et al., 2019; Berends et al., 2021). Nevertheless, lowland rainforests remained the dominant biome across Amazonia, and river-associated wetlands may have benefitted from higher-than-modern sea-level stands (Irion et al., 2010; de Boer et al., 2014) (Fig. 8E–G).

Following the MPT, with the onset of the large-amplitude, long-period glacial-interglacial cycles of the late Pleistocene, lowland vegetation underwent its most significant compositional changes of the entire record (Fig. 4; 6). The periodically lower sea levels after 700 ka are correlated with a diminished extent of wetland vegetation. Although sea level change likely would not have a significant impact on rivers farther inland (Pupim et al., 2019), it plausibly may have influenced the eastern section of the Amazon Basin (Irion et al., 2010), affecting herbaceous wetland taxa. Overall vegetation change does not appear to have become synchronized with glacial-interglacial climate variations until ca. 400 ka, after the Mid-Bruhnes Event (Lisiecki and Raymo, 2005; Barth et al., 2018). Despite strong global climate, sea level, and CO_2 oscillations between 800 and 400 ka (Lisiecki and Raymo, 2005; Lüthi et al., 2010; Willeit et al., 2019; Berends et al., 2021), the nature of the pollen record of CDH-79 precludes accurate evaluation of vegetation change, possibly due to the low influx of terrigenous material (i.e. the low accumulation rate and pollen concentration) during this interval (Fig. 3B; D).

During the past 400 ka, Amazonian lowland vegetation was characterized by synchronous variation between high-diversity tropical rainforest during interglacial stages and mixed rainforest, including evergreen and seasonally deciduous elements, during glacial stages (Fig. 8). Higher interglacial temperatures and particularly atmospheric CO_2 levels apparently favored rapid growth of rainforest trees, even in potential relative dryness (Maksic et al.,

2022). In particular, it appears that at the onset of MIS 9 and 7, rainforests expanded rapidly coincident with increasing CO_2 levels. Ongoing interglacial conditions and a small decrease of CO_2 co-occurred with a drop in evergreen rainforests, while tropical seasonal and dry forests presumably persisted in the drier and more seasonal climatic zones within the drainage basin (Fig. 5B; C; Supplementary Table 3). Our observations support the hypothesis that high CO_2 is an important driver for evergreen Amazonia (Bueno et al., 2017).

As we observe prominent pulses of open vegetation types (e.g. STEP; Marchant et al., 2009) in the CDH-79 record during both glacial and interglacial stages, no interpretation of the precipitation patterns over Amazonia is conclusive. This might be the result of contributions from disparate sources within the large and heterogeneous Amazon catchment. Instead of an expansion of savanna (TDRF), however, the apparently drier regions in eastern Amazonia remained largely forested during all recorded glacial stages in CDH-79. Shifting compositions towards a seasonal forest (TSFO) implies an extended dry season that favors sclerophyllous and deciduous trees in parts of lowland Amazonia (Table 1). This forest type may have undergone sufficient expansion during glacial stages to periodically establish a biotic corridor with northeastern Brazil, which itself may have exhibited wetter conditions during the last glacial stage (Piacsek et al., 2021) and, presumably, previous glacial stages as well.

Whereas some vegetation model experiments indicate a limited impact of low CO_2 during glacial stages on Amazonian vegetation (Beerling and Mayle, 2006; Sato et al., 2021), others suggest a significant control (Scheff et al., 2017; Maksic et al., 2022). From a plant physiological point of view, lower CO_2 favors the growth of C4 plants over C3 plants, making the former more competitive during glacial stages (Beerling and Osborne, 2006; Murphy and Bowman, 2012; Bellasio et al., 2018). Although lower CO_2 levels could promote an expansion of grass vegetation by inhibiting tree growth (Murphy and Bowman, 2012), our reconstructions do not show strong vegetation turnover during any glacial stage in Amazonia. The switch from a rainforest to savanna is controlled by multiple variables and feedback mechanisms, particularly in South America, where neither mean annual precipitation nor dry season soil saturation appear to be good indicators for the distribution of modern forest vegetation relative to savanna (Murphy and Bowman, 2012). In any case, the CDH-79 dataset suggests glacial transitions to more tropical seasonal forests (Maksic et al., 2022) and an opening of the forest canopy during some time during the year (Cowling et al., 2001) particularly during the last 400 ka.

6. Conclusion

The marine palynological record from CDH-79 records the history of Amazonian biomes for the past 1800 kyr exceeding the temporal length of previous records by an order of magnitude. The biome reconstruction reveals a continuous presence of a highly diverse tropical rainforest in large areas of the Amazon drainage basin since the middle Pleistocene. During the exceptionally warm interglacial stages MIS 33 and 31 (i.e. early MPT), the tropical rainforest expanded across Amazonia. Subsequently, global climate cooling and CO_2 decrease led to a forest compositional change towards colder and possibly drier forest elements. A major change occurred at the end of the MPT around 800–700 ka, probably marked by a strong reduction of the eastern Amazonian wetlands, partly driven by falling of long-term mean sea level. Global climate and Amazonian vegetation changed synchronously during the last 400 ka of intensified glacial-interglacial cycles. High temperature and CO_2 levels during interglacial stages likely favored the expansion of lowland tropical rainforest while during glacial stages, tropical seasonal forests increased and even dominated at certain times. Our data show no indication of a significant expansion of savanna-like vegetation in the Amazon River drainage basin during the entire 1800 kyr record. This study is the first continuous record of Amazonian lowland vegetation as seen from offshore the Brazilian coast spanning the last 1800 ka. It shows important events of Pleistocene climate history such as the Mid-Pleistocene Transition and the Mid-Bruhnes Event. In addition, it raises questions on the migration route and first occurrence of *Alnus* towards South America. Our study gives insights into the response of Amazonian vegetation to the strengthening of glacial-interglacial cycles and supports CO_2 as a key driver of Amazonian vegetation distribution. None-the-less, additional regional studies using quantitative methods and records with higher temporal resolution are necessary to further capture the magnitude of vegetation and climate change in the Amazonian realm.

Author contributions

A.K.K. performed the palynological interpretation and biome reconstruction and prepared the manuscript. T.K.A. assisted in the biome reconstruction and interpretation and helped to prepare, edit and revise the manuscript. J.Q.F. provided the isotopic analysis and was active in discussion, interpretation and revising the draft. C.M.C. supervised the discussion and interpretation and assisted in the review and editing of the manuscript. D.A.W. was involved in the palynological discussion and helped the reviewing and editing of the manuscript. F.F. sampled the core, established the age model and was involved in the discussion, interpretation and preparation of the manuscript. A.O.S. sampled the core and was involved in the discussion and interpretation of the manuscript. C.G.S., C.R. and G.S.D. assisted during the fieldwork and with reviewing and editing. F.C.W. assisted in the discussion and interpretation of the data. S.C.F. and P.A.B. supervised the study, assisted in the discussion and interpretation of the data and the reviewing and editing of the manuscript.

Declaration of competing interest

The authors declare that they have no known competing financial interests or personal relationships that could have appeared to influence the work reported in this paper.

Data availability

All data used is available in the provided supplementary material

Acknowledgements

Funding was provided by grants from FAPESP 2014/05582–0, 2012/50260–6, 2015/18314–7 to A.K.K.; and from NSF (EAR-1812681 and OCE-0823650) to P.A.B.; and NSF (EAR-1812857) to S.C.F.. This research was partially funded through the 2019–2020 BiodivERsA joint call for research proposals, under the BiodivClim ERA-Net COFUND program, and with the funding organization FAPESP (grant 2019/24349–9). C.M.C. acknowledges the financial support from FAPESP (grant 2018/15123–4) and CNPq (grant 312458/2020–7). F.F. has the support of the Brazilian agency CAPES [grant numbers 88882.151083/2017–01, and 88881.185132/2018–01. T.K.A. acknowledges the financial support from FAPESP (grant 2019/19948–0). D.W. was supported by the U.S. Geological Survey Land Change Science/Climate Research & Development Program. Any use of trade, firm, or product names is for descriptive purposes only and does not imply endorsement by the U.S.

Government We thank the officers, crew, and support personnel of the R/V Knorr and WHOI. We especially acknowledge the long-core coring team. The innovative design work, tireless deck work, and leadership of James Broda were indispensable. The work was made possible by the cooperation of the Brazilian navy and the government of Brazil. We acknowledge Frank Mayle (University of Reading) for access to his pollen collection.

Appendix A. Supplementary data

Supplementary data to this article can be found online at https://doi.org/10.1016/j.quascirev.2022.107867.

References

Abe-Ouchi, A., Saito, F., Kageyama, M., Craconnot, P., Harrison, S.P., Lambeck, K., Otto-Blisner, L., Peltier, W.R., Tarasov, L., Peterschmitt, J.-Y., Takahashi, K., 2015. Ice-sheet configuration in the CMIP5/PMIP3 last glacial maximum experiments. Geosci. Model Dev. (GMD) 8, 3621–3637. https://doi.org/10.5194/gmd-8-3621-2015.

Absy, M.L., Cleef, A., Fournier, M., Martin, L., Servant, M., Sifeddine, A., da Silva, F., Soubiès, F., Suguio, K., Turcq, B., van der Hammen, T., 1991. Mise en évidence de quatre phases d'ouverture de la forêt dense dans le sud-est de L'Amazonie au cours des 60,000 dernières années. Première comparaison avec d'autres régions tropicales. Comptes Rendus de l'Academie des Sciences, Paris, Series II 312, 673–678. ISSN 0249-6305.

Akabane, T.K., Oliveira, P.E., Sawakuchi, A.O., Chiessi, C.M., Kern, A.K., Pinaya, J.L.D., Cennantini, G.C.T., 2020. Modern pollen signatures of the Solimões-Amazon River and its major tributaries. Palaeogeogr. Palaeoclimatol. Palaeoecol. 553, 109802. https://doi.org/10.1016/j.palaeo.2020.109802.

Allen, J.R.M., Forrest, M., Hickler, T., Singarayer, J.S., Valdes, P.J., Huntley, B., 2020. Global vegetation patterns of the past 140,000 years. J. Biogeogr. 47, 2073–2090. https://doi.org/10.1111/jbi.13930.

Allison, M.A., Lee, M.T., Ogston, A.S., Aller, R.C., 2000. Origin of Amazon mudbanks along the northeastern coast of South America. Mar. Geol. 163, 241–256. https://doi.org/10.1016/S0025-3227(99)00120-6.

Altolaguirre, Y., Bruch, A.A., Gibert, L., 2020. A long early Pleistocene pollen record from baza basin (SE Spain): major contributions to the palaeoclimate and palaeovegetation of southern europe. Quat. Sci. Rev. 231, 106199. https://doi.org/10.1016/j.quascirev.2020.106199.

Baker, P.A., Fritz, S.C., 2015. Nature and causes of Quaternary climate variation of tropical South America. Quat. Sci. Rev. 124, 31–47. https://doi.org/10.1016/j.quascirev.2015.06.011.

Baker, P.A., Fritz, S.C., Battisti, D.S., Dick, C.W., Vargas, O.M., Asner, G.P., Martin, R.E., Wheatley, A., Prates, I., 2020. Beyond refugia: new insights on quaternary climate variation and the evolution of biotic diversity in tropical SouthSouth America. In: Rull, V., Carnaval, A. (Eds.), Neotropical Diversification: Patterns and Processes. Fascinating Life Sciences. Springer, Cham. https://doi.org/10.1007/978-3-030-31167-4_3.

Barth, A.M., Clark, P.U., Bill, N.S., He, F., Pisias, N.G., 2018. Climate evolution across the mid-brunhes transition. Clim. Past 14, 2071–2087. https://doi.org/10.5194/cp-14-2071-2018.

Barros, M.H.M.R., Luz, C.F.P., Albuquerque, P.M.C., 2013. Pollen analysis of geopropolis of melipona (melikerria) fasciculate Smith, 1854 (meliponini, apidae, hymenoptera) in areas of restinga, Cerrado and flooded fields in the state of maranhão, Brazil. Grana 52, 81–92. https://doi.org/10.1080/00173134.2013.765909.

Beerling, D.J., Mayle, F.E., 2006. Contrasting effects of climate and CO2 on Amazonian ecosystems since the last glacial maximum. Global Change Biol. 12, 1977–1984. https://doi.org/10.1111/j.1365-2486.2006.01228.x.

Beerling, D.J., Osborne, C.P., 2006. The origin of the savanna biome. Global Change Biol. 12, 2023–2031. https://doi.org/10.1111/j.1365-2486.2006.01239.x.

Bellasio, C., Quirk, J., Beerling, D.J., 2018. Stomatal and non-stomatal limitations in savanna trees and C4 grasses grown at low, ambient and high atmospheric CO_2. Plant Sci. 274, 181–192. https://doi.org/10.1016/j.plantsci.2018.05.028.

Bell, D.B., Jung, S.J.A., Kroon, D., 2015. The Plio-Pleistocene development of Atlantic deep-water circulation and its influence on climate trends. Quat. Sci. Rev. 123, 265–282. https://doi.org/10.1016/j.quascirev.2015.06.026.

Berends, C.J., de Boer, B., van de Wal, R.S.W., 2021. Reconstructing the evolution of ice sheets, sea level, and atmospheric CO_2 during the past 3.6 million years. Clim. Past 17, 361–377. https://doi.org/10.5194/cp-17-361-2021.

Blodgett, T.A., 1998. Erosion Rate on the NE Escarpment of the Eastern Cordillera, Bolivia Derived from Aerial Photographs and Thematic Mapper Images. Ph.D. Thesis. Cornell University, Ithaca, NY, USA.

Böning, C.W., Kröger, J., 2005. Seasonal variability of deep currents in the equatorial Atlantic: a model study. Deep-Sea Res. I 52, 99–121. https://doi.org/10.1016/j.dsr.2004.06.015.

Brown, C.A., 2008. Palynological Techniques. American Association of Stratigraphic Palynologists Foundation, Dallas, p. 137.

Brown, A.D., Grau, H.R., Malizia, L.R., Grau, A., 2001. Argentina. In: Kappelle, M., Brown, A.D. (Eds.), Bosques Nublados del Neotropico. Editorial INBio, Santo Domingo de Heredia, Costa Rica, pp. 623–659.

Buckley, M.W., Marshall, J., 2016. Observations, inferences, and mechanisms of atlantic meridional overturning circulation variability: a review. Rev. Geophys. 54, 5–63. https://doi.org/10.1002/2015RG000493.

Bueno, M.L., Pennington, R.T., Dexter, K.G., Kamino, L.Y.Y., Pontara, V., Neves, D.M., Ratter, J.A., Oliveria-Filho, A.T., 2017. Effects of Quaternary climatic fluctuations on the distribution of Neotropical savanna tree species. Ecography 40, 403–414. https://doi.org/10.1111/ecog.01860.

Burn, M.J., Mayle, F.E., 2008. Palynological differentiation between genera of the Moraceae family and implications for Amazonian palaeoecology. Rev. Palaeobot. Palynol. 149, 187–201. https://doi.org/10.1016/j.revpalbo.2007.12.003.

Burn, M., Mayle, F., Killeen, T., 2010. Pollen-based differentiation of Amazonian rainforest communities and implications for lowland palaeoecology in tropical South America. Palaeogeogr. Palaeoclimatol. Palaeoecol. 295, 1–18. https://doi.org/10.1016/j.palaeo.2010.05.009.

Burnham, R.J., Graham, A., 1999. The history of neotropical vegetation: new developments and status. Ann. Mo. Bot. Gard. 86, 546–589. https://www.jstor.org/stable/2666185.

Bush, M., 2002. On the interpretation of fossil Poaceae pollen in the lowland humid neotropics. Palaeogeogr. Palaeoclimatol. Palaeoecol. 177, 5–17. https://doi.org/10.1016/S0031-0182(01)00348-0.

Bush, M.B., Weng, M.B., 2007. Introducing a new (freeware) tool for palynology. J. Biogeogr. 34, 377–380. https://doi.org/10.1111/j.1365-2699.2006.01645.x.

Chalk, T.B., Hain, M.P., Foster, G.L., Rohling, E.J., Sexton, P.F., Badger, M.P.S., Cherry, S.G., Hasenfratz, A.P., Haug, G.H., Jaccard, S.L., Martínez-García, A., Pälike, H., Pancost, R.D., Wilson, P.A., 2017. Causes of ice age intensification across the Mid-Pleistocene Transition. Proc. Natl. Acad. Sci. USA 114, 13114–13119. https://doi.org/10.1073/pnas.1702143114.

Clark, P.U., Archer, D., Pollard, D., Blum, J.D., Rial, J.A., Brovkin, V., Mix, A.C., Pisias, N.G., Roy, M., 2006. The middle Pleistocene transition: characteristics, mechanisms, and implications for long-term changes in atmospheric pCO2. Quat. Sci. Rev. 25, 3150–3184. https://doi.org/10.1016/j.quascirev.2006.07.008.

Clark, P.U., Dyke, A.S., Shakun, J.D., Carlson, A.E., Clark, J., Wohlfarth, B., Mitrovica, J.X., Hostetler, S.W., McCabe, A.M., 2009. The last glacial maximum. Science 325, 710–714. https://doi.org/10.1126/science.1172873.

Clark, T.B., Hain, M.P., Foster, G.L., Rohling, E.J., Sexton, P.F., Badger, M.P.S., Cherry, S.G., Hasenfratz, A.F., Haug, G.H., Jaccard, S.L., Martínez-García, A., Pälike, H., Pancost, R.D., Wilson, P.A., 2017. Causes of ice age intensification across the Mid-Pleistocene Transition. Proc. Natl. Acad. Sci. USA 114, 13114–13119. https://doi.org/10.1073/pnas.1702143114.

Cohen, M.C.L., Rossetti, D.F., , PessɛNda, L.C.R., Friaes, Y.S., Oliveira, P.E., 2014. Late Pleistocene glacial forest of humaitá—western Amazonia. Palaeogeogr. Palaeoclimatol. Palaeoecol. 415, 37–47. https://doi.org/10.1016/j.palaeo.2013.12.025.

Colinvaux, P., de Oliveira, P.E., Moreno, P.J.E., 1999. Amazon: Pollen Manual and Atlas. CRC Press, p. 344.

Colinvaux, P.A., De Oliveira, P.E., Moreno, J.E., Miller, M.C., Bush, M.B., 1996. A long pollen record from lowland Amazonia: forest and cooling in glacial times. Science 274, 85–88. https://doi.org/10.1126/science.274.5284.85.

Colinvaux, P.A., De Oliveira, P.E., Bush, M.B., 2000. Amazon and Neotropical plant communities on glacial time scales: the failure of the aridity and refuge hypotheses. Quat. Sci. Rev. 19, 141–169. https://doi.org/10.1016/S0277-3791(99)00059-1.

Cowling, S.A., Maslin, M.A., Sykes, M.T., 2001. Paleovegetation simulations of lowland Amazonia and implications for neotropical allopatry and speciation. Quat. Res. 55, 140–149. https://doi.org/10.1006/qres.2000.2197.

Crivellari, S., Chiessi, C.M., Kuhnert, H., Häggi, C., Mollenhauer, G., Hefter, J., Portilho-Ramos, R., Schefuß, E., Mulitzer, S., 2019. Thermal response of the western tropical atlantic to slowdown of the atlantic meridional overturning circulation. Earth Planet Sci. Lett. 519, 120–129. https://doi.org/10.1016/j.epsl.2019.05.006.

Cuatrecasas, J., 1958. Aspectos de la vegetación natural de Colombia. Revista Academia Colombiana Ciencias Exactas Físicas Naturales 10, 221–269.

Curry, W.B., Cullen, J.L., 1997. Carbonate production and dissolution in the western equatorial Atlantic during the last 1 M.y. Proc. ODP Sci. Results 154, 189–199.

D'Apolito, C., Absy, M.L., Latrubesse, E.M., 2013. The Hill of Six Lakes revisited: new data and re-evaluation of a key Pleistocene Amazon site. Quat. Sci. Rev. 76, 140–155. https://doi.org/10.1016/j.quascirev.2013.07.013.

Daly, D.C., Mitchell, J.D., 2000. Lowland vegetation of tropical South America – an overview. In: Lentz, D. (Ed.), Imperfect Balance: Landscape Transformations in the Pre-columbian Americas. Columbia University Press, New York, pp. 391–454.

Damuth, J.E., Flood, R.D., Pirmez, C., Manley, P.I., 1995. Architectural elements and depositional processes of Amazon deep-sea Fan imaged by long-range sidescan sonar (GLORIA), bathymetric swath-mapping (Sea Beam), high-resolution seismic and piston-core data. In: Pickering, K.T., Hiscott, R.N., Kenyon, N.H., Ricci Lucchi, F., Smith, R.D.A. (Eds.), Atlas of Deep Water Environments. Springer, Dordrecht. https://doi.org/10.1007/978-94-011-1234-5_19.

da Silva, J.M.C., Rylands, A.B., Fonseca, G.A.B., 2005. The fate of the Amazonian areas of endemism. Conserv. Biol. 19, 689–694. http://www.jstor.org/stable/3591055.

da Silva, E.F., Lopes, K.S., Alves, R., Medeiros Carreira, L.M., da Silva, D.F., Araújo Romeiro, L., Batista, W.F., Rodrigues, T.M., Secco, R.S., Guimarães, J.T.F., 2020. Hydroclimate influences on modern pollen rain of upland southeastern Amazonia. Holocene 30, 721–732. https://doi.org/10.1177/0959683619895586.

de Boer, B., Lourens, L., van de Wal, R., 2014. Persistent 400,000-year variability of Antarctic ice volume and the carbon cycle is revealed throughout the Plio-

Pleistocene. Nat. Commun. 5, 2999. https://doi.org/10.1038/ncomms3999.
DePaolo, D.J., 1981. A neodymium and strontium isotopic study of the Mesozoic calc-alkaline granitic batholiths of the Sierra Nevada and Peninsular Ranges, California. J. Geophys. Res. 86, 10470–10488. https://doi.org/10.1029/JB086iB11p10470.
de Wet, G.A., Castañeda, I.S., DeConto, R.M., Brigham-Grette, J., 2016. A high-resolution mid-Pleistocene temperature record from Arctic Lake El'gygytgyn: a 50 kyr super interglacial from MIS 33 to MIS 31? Earth Planet Sci. Lett. 436, 56–63. https://doi.org/10.1016/j.epsl.2015.12.021.
Doher, L.I., 1980. Palynomorph preparation procedures currently used in the paleontology and stratigraphy laboratories. U.S. Geological Survey, Geological Survey Circular 830, 1–28.
Douda, J., Doudová, J., Drašnarová, A., Kuneš, P., Hadincová, V., Krak, K., Zákravský, P., Mandák, B., 2014. Migration patterns of subgenus Alnus in europe since the last glacial maximum: a systematic review. PLoS One 9, e88709. https://doi.org/10.1371/journal.pone.0088709.
Dupont, L.M., Donner, B., Schneider, R., Weger, G., 2001. Mid-Pleistocene environmental change in tropical Africa began as early as 1.05 Ma. Geology 29, 195–198. https://doi.org/10.1130/0091-7613(2001)029<0195:MPECIT>2.0.CO, 2.
Eiten, G., 1972. Cerrado vegetation of Brazil. Bot. Rev. 38, 201–341. http://www.jstor.org/stable/4353829.
Ericson, D.B., Wollin, G., 1968. Pleistocene climates and chronology in deep-sea sediments. Science 162, 1227–1234. https://doi.org/10.1126/science.162.3859.1227.
Faegri, K., Iversen, J., 1975. Textbook of Pollen Analysis. Hafner Press, New York, p. 295.
Ferreira, F., Silva, C.G., Oliveira, A.S., Chiessi, C.M., Kern, A.K., Baker, P.A., Dwyer, G., Rigsby, C.A., Huang, E., Tian, J., 2021. Biochronostratigraphy of the western equatorial Atlantic for the last 1.93 Ma. Quat. Int. 598, 24–37. https://doi.org/10.1016/j.quaint.2021.04.042.
Fischer, J., Schott, F.A., 1997. Seasonal transport variability of the deep western boundary current in the equatorial atlantic. J. Geophys. Res. 102, 27751–27769. https://doi.org/10.1016/j.dsr.2004.06.015.
Flood, R., Piper, D.J.W., 1997. Amazon fan sediments: the relationship to equatorial climate change, continental denudation, and sea level fluctuations. Proc. Ocean Drill. Progr. Sci. Results 155.
Fontes, A., Cordeiro, R.C., Martins, G.S., Behling, H., Turcq, B., Sifeddine, A., Seoane, J.C.S., Moreira, L.S., Rodrigues, R.A., 2017. Paleoenvironmental dynamics in South Amazonia, Brazil, during the last 35,000 years inferred from pollen and geochemical records of Lago do Saci. Quat. Sci. Rev. 173, 161–180. https://doi.org/10.1016/j.quascirev.2017.08.021.
Fournier, L.A., 2002. *Alnus acuminata* kunth in H.B.K. In: Vozzo, J. (Ed.), Tropical Tree Seed Manual. USDA Forest Service, pp. 289–291. Available at: http://www.rngr.net/publications/ttsm/species.
Fratantoni, D., Johns, W.E., Townsend, T.L., Hurlburt, H.E., 2000. Low-latitude circulation and mass transport pathways in a model of the tropical Atlantic Ocean. J. Phys. Oceanogr. 30, 1944–1966. https://doi.org/10.1175/1520-0485(2000)030<1944:LLCAMT>2.0.CO, 2.
Furley, P., 2007. Tropical forest of the lowlands. In: Veblen, T.T., Young, K.R., Orme, A.R. (Eds.), The Physical Geography of South America, pp. 135–158. https://doi.org/10.1093/oso/9780195313413.003.0017.
Germeraad, J.H., Hopping, C.A., Muller, J., 1968. Palynology of Tertiary sediments from tropical areas. Rev. Palaeobot. Palynol. 6, 189–348. https://doi.org/10.1016/0034-6667(68)90051-1.
Giesecke, T., Ammann, B., Brande, A., 2014. Palynological richness and evenness: insights from the taxa accumulation curve. Veg. Hist. Archaeobotany 23, 217–228. https://doi.org/10.1007/s00334-014-0435-5.
González, C., Lupont, L.M., 2009. Tropical salt marsh succession as sea-level indicator during Heinrich events. Quat. Sci. Rev. 28, 939–946. https://doi.org/10.1016/j.quascirev.2008.12.023.
Gosling, W.D., Mayle, F.E., Tate, N.J., Killeen, T.J., 2009. Differentiation between Neotropical rainforest, dry forest, and savannah ecosystems by their modern pollen spectra and implications for the fossil pollen record. Rev. Palaeobot. Palynol. 153, 70–85. https://doi.org/10.1016/j.revpalbo.2008.06.007.
Govin, A., Braconnot, P., Capron, E., Cortijo, E., Duplessy, J.-C., Jansen, E., Labeyrie, L., Landais, A., Marti, O., Michel, E., Mosquet, E., Risebrobakken, B., Swingedouw, D., Waelbroeck, C., 2012. Persistent influence of ice sheet melting on high northern latitude climate during the early Last Interglacial. Clim. Past 8, 483–507. https://doi.org/10.5194/cp-8-483-2012.
Govin, A., Chiessi, C.M., Zabel, M., Sawakuchi, A.O., Heslop, D., Hörner, T., Zhang, Y., Mulitza, S., 2014. Terrigenous input off northern South America driven by changes in Amazonian climate and the North Brazil Current retroflection during the last 250 ka. Clim. Past 10, 843–862. https://doi.org/10.5194/cp-10-843-2014.
Graham, A., 1976. Studies in neotropical paleobotany. II the miocene communities of veracruz, Mexico. Ann. Mo. Bot. Gard. 63, 787–842. https://doi.org/10.2307/2395250.
Graham, A., 1999. The Tertiary history of the northern temperate element in the northern Latin American biota. Am. J. Bot. 86, 32–38. https://doi.org/10.2307/2656952.
Haberle, S., 1997. Upper Quaternary vegetation and climate history of the Amazon Basin: correlating marine and terrestrial pollen records. Proc. Ocean Drill. Progr. Sci. Results 155, 381–396. https://doi.org/10.2973/odp.proc.sr.155.225.1997.
Haffer, J., 1969. Speciation in Amazonian forest birds. Science 165, 131–137. https://doi.org/10.1126/science.165.3889.131.
Häggi, C., Sawakuchi, A.O., Chiessi, C.M., Muliza, S., Mollenhauer, G., Sawakuchi, H.O., Baker, P.A., Zabel, M., Schnefuß, E., 2016. Origin, transport and deposition of leaf-wax biomarkers in the Amazon Basin and the adjacent Atlantic. Geochem. Cosmochim. Acta 192, 149–165. https://doi.org/10.1016/j.gca.2016.07.002.
Häggi, C., Chiessi, C.M., Merkel, U., Mulitza, S., Prange, M., Schulz, M., Schefuß, E., 2017. Response of the Amazon rainforest to late Pleistocene climate variability. Earth Planet Sci. Lett. 479, 50–59. https://doi.org/10.1016/j.epsl.2017.09.013.
Halloy, S., Beck, S.G., Ledezma, J.C., 2008. South America - central andean grasslands (páramo, puna) and high andean (central and southern perú, western Bolivia, northern Chile and northwestern Argentina). In: A Compendium of Regional Templates on the Status of Temperate Grasslands Conservation and Protection. workshop report, Vancouver, pp. 97–108.
Hammer, Ø., Harper, D.A.T., Ryan, P.D., 2001. PAST: paleontological statistics software package for education and data analysis. Palaeontol. Electron. 4, 9.
Harris, S.E., Mix, A.C., 1999. Pleistocene precipitation balance in the Amazon Basin recorded in deep sea sediments. Quat. Res. 51, 14–26. https://doi.org/10.1006/qres.1998.2008.
Hermanowski, B., Costa, M.L., Carvalho, A.T., Behling, H., 2012. Palaeoenvironmental dynamics and underlying climatic changes in southeast Amazonia (Serra Sul dos Carajás, Brazil) during the late Pleistocene and Holocene. Palaeogeogr. Palaeoclimatol. Palaeoecol. 365–366, 227–246. https://doi.org/10.1016/j.palaeo.2012.09.030.
Hess, L.L., Melack, J.M., Affonso, A.G., Barbosa, G., Gastil-Buhl, M., Novo, E.M.L.M., 2015. Wetlands of the lowland Amazon Basin: extent, vegetative cover, and dual-season inundated area as mapped with JERS-1 synthetic aperture radar. Wetlands 35, 745–756. https://doi.org/10.1007/s13157-015-0666-y.
Homeier, J., Werner, F.A., Gradstein, S.R., Breckle, S.-W., Richter, M., 2008. Potential vegetation and floristic composition of Andean forests in South Ecuador, with a focus on the RBSF. In: Beck, E., Bendix, J., Kottke, I., Makeschin, F., Mosandl, R. (Eds.), Gradients in a Tropical Mountain Ecosystem of Ecuador. Springer, Berlin, Heidelberg, pp. 87–100.
Hönisch, B., Hemming, N.G., Archer, D., Siddall, M., McManus, J.F., 2009. Atmospheric carbon dioxide concentration across the Mid-Pleistocene Transition. Science 324, 1551–1554. https://doi.org/10.1126/science.1171477.
Hooghiemstra, H., 1984. Vegetational and climatic history of the high plain of Bogotá, Colombia. Diss. Bot. 79, 1–368. J. Cramer, Vaduz.
Hooghiemstra, H., Ran, E.T.H., 1994. Late Pliocene– Pleistocene high resolution pollen sequence of Colombia: an overview of climatic change. Quat. Int. 21, 63–80. https://doi.org/10.1016/1040-6182(94)90021-3.
Hooghiemstra, H., Cleef, A.M., 1995. Pleistocene climatic change, environmental and generic dynamics in the north Andean montane forest and paramo. In: Churchill, S.P., et al. (Eds.), Biodiversity and Conservation of Neotropical Montane Forests. The New York Botanical Garden, New York, pp. 35–49.
Hooghiemstra, H., Flantua, S.G.A., 2019. Colombia in the Quaternary: an overview of environmental and climatic change. In: Gómez, J., Pinilla–Pachon, A.O. (Eds.), The Geology of Colombia, Volume 4 Quaternary. Servicio Geológico Colombiano, Publicaciones Geológicas Especiales, Bogotá, p. 52. https://doi.org/10.32685/pub.esp.38.2019.02, 38.
Hooghiemstra, H., Sarmiento Pérez, G., Torres Torres, V., Berrio, J.-C., Lourens, L., Flantua, S., 2022. 60 years of scientific deep drilling in Colombia: the North Andean guide to the Quaternary. Sci. Drill. 30, 1–15. https://doi.org/10.5194/sd-30-1-2022.
Hoorn, C., 1997. Palynology of the Pleistocene glacial/interglacial cycles of the Amazon Fan (holes 940A, 944A, and 946A). In: Flood, R.D., Piper, D.J.W., Klaus, A., Peterson, L.C. (Eds.), Proc. Ocean Drill. Progr. Sci. Results 155, 397–409.
Hoorn, C., Bogotá-A, G.R., Romero-Baez, M., Lammertsma, E.I., Flantua, S.G.A., Dantas, E.L., Dino, R., do Carmo, D.A., Chemale Jr., F., 2017. The Amazon at sea: onset and stages of the Amazon River from a marine record, with special reference to Neogene plant turnover in the drainage basin. Global Planet. Change 153, 51–65. https://doi.org/10.1016/j.gloplacha.2017.02.005.
Höppner, N., Lucassen, F., Chiessi, C.M., Sawakuchi, A.O., Kasemann, S., 2018. Holocene provenance shift of suspended particulate matter in the Amazon River basin. Quat. Sci. Rev. 190, 66–80. https://doi.org/10.1016/j.quascirev.2018.04.021.
Howe, J.N.W., Piotrowski, A.M., Noble, T.L., Mulitza, S., Chiessi, C.M., Bayon, G., 2016. North Atlantic deep water production during the last glacial maximum. Nat. Commun. 7, 11765. https://doi.org/10.1038/ncomms11765.
Irion, G., Mello, J.A.S.N., Morais, J., Piedade, M.T.F., Junk, W.J., Garming, L., 2010. Development of the Amazon valley during the middle to late quaternary: sedimentological and climatological observations. In: Junk, W., Piedade, M., Wittmann, F., Schöngart, J., Parolin, P. (Eds.), Amazonian Floodplain Forests, Ecological Studies, vol. 210. Springer, Dordrecht, pp. 27–42. https://doi.org/10.1007/978-90-481-8725-6_2.
Izumi, K., Lézine, A.-M., 2016. Pollen-based biome reconstructions over the past 18,000 years and atmospheric CO_2 impacts on vegetation in equatorial mountains of Africa. Quat. Sci. Rev. 152, 93–103. https://doi.org/10.1016/j.quascirev.2016.09.023.
Jacobsen, S.B., Wasserburg, G.J., 1980. Sm-Nd isotopic evolution of chondrites. Earth Planet Sci. Lett. 50, 139–155. https://doi.org/10.1016/0012-821X(80)90125-9.
Jantz, N., Homeier, J., León-Yánez, S., Moscoso, A., Behling, H., 2013. Trapping pollen in the tropics — comparing modern pollen rain spectra of different pollen traps and surface samples across Andean vegetation zones. Rev. Palaeobot. Palynol. 193, 57–69. https://doi.org/10.1016/j.revpalbo.2013.01.011.

Jennerjahn, T.C., Ittekkot, V., Arz, H.W., Behling, H., Pätzold, J., Wefer, G., 2004. Asynchronous terrestrial and marine signals of climate change during Heinrich Events. Science 306, 2236–2239. https://doi.org/10.1126/science.1102490.
Juggins, S., 2020. Rioja: Analysis of Quaternary Science Data 26. R package version 0.9. https://cran.r-project.org/package=rioja.
Kenkel, N.C., 2006. On selecting an appropriate multivariate analysis. Can. J. Plant Sci. 86, 663–676. https://doi.org/10.4141/P05-164.
Latrubesse, E.M., Cozzuol, M., da Silva-Caminha, S.A.F., Rigsby, C.A., Absy, M.L., Jaramillo, C., 2010. The late miocene paleogeography of the Amazon Basin and the evolution of the Amazon River system. Earth Sci. Rev. 99, 99–124. https://doi.org/10.1016/j.earscirev.2010.02.005.
Ledru, M.-P., Bertaux, J., Sifeddine, A., 1998. Absence of Last Glacial Maximum records in lowland tropic forests. Quat. Res. 49, 233–237. https://doi.org/10.1006/qres.1997.1953.
Legendre, P., Birks, H.J.B., 2012. From classical to canonical ordination. In: Birks, H., Lotter, A., Juggins, S., Smol, J. (Eds.), Tracking Environmental Change Using Lake Sediments, Developments in Paleoenvironmental Research, vol. 5. Springer, Dordrecht. https://doi.org/10.1007/978-94-007-2745-8_8.
Lentz, S.J., 1995. Seasonal variations in the Amazon plume structure inferred from historical hydrographic data. J. Geophys. Res. 100, 2391–2400. https://doi.org/10.1029/94JC01847.
Li, Y.-C., Xu, Q.-H., Yang, X.-L., Chen, H., Lu, X.-M., 2005. Pollen-vegetation relationship and pollen preservation on the Northeastern Qinghai-Tibetan Plateau. Grana 44, 160–171. https://doi.org/10.1080/00173130500230608.
Lima, W.J.S., Cohen, M.C.L., Rossetti, D.F., França, M.C., 2018. Late Pleistocene glacial forest elements of Brazilian Amazonia. Palaeogeogr. Palaeoclimatol. Palaeoecol. 490, 617–628. https://doi.org/10.1016/j.palaeo.2017.11.050.
Lisiecki, L.E., Raymo, M.E., 2005. A Pliocene-Pleistocene stack of 57 globally distributed benthic d18O records. Paleoceanography 20, 1–17. https://doi.org/10.1029/2004PA001071.
Londoño, C., Cleef, A., Madriñán, S., 2014. Angiosperm flora and biogeography of the páramo region of Colombia, Northern Andes. Flora 209, 81–87. https://doi.org/10.1016/j.flora.2013.11.006.
Lüthi, D., Bereiter, B., Stauffer, B., Winkler, R., Schwander, J., Kindler, P., Leuenberger, M., Kipfstuhl, S., Carpon, E., Landais, A., Fischer, H., Stocker, T.F., 2010. CO_2 and O_2/N_2 variations in and just below the bubble–clathrate transformation zone of Antarctic ice cores. Earth Planet Sci. Lett. 297, 226–233. https://doi.org/10.1016/j.epsl.2010.06.023.
Macsotay, O., 2005. The humboldt channel: early Pleistocene extensional graben through eastern Venezuela and trinidad. Transactions of the 16th caribbean geological conference, Barbados. Caribb. J. Earth Sci. 39, 83–91.
Meade, R.H., 1994. Suspended sediments of the modern Amazon and Orinoco rivers. Quat. Int. 21, 29–39. https://doi.org/10.1016/1040-6182(94)90019-1.
Maksic, J., Venancio, I.M., Shimizu, M.H., Chiessi, C.M., Piacsek, P., Sampaio, G., Cruz, F.W., Alexandre, F.F., 2022. Brazilian biomes distribution: past and future Palaeogeogr. Palaeoclimatol. Palaeoecol. 585, 110717. https://doi.org/10.1016/j.palaeo.2021.110717.
Marchant, R., Cleef, A., Harrison, S.P., Hooghiemstra, H., Markgraf, V., van Boxel, J., Ager, T., Almeida, L., Anderson, R., Baied, C., Behling, H., Berrio, J.C., Burbridge, R., Björck, S., Byrne, R., Bush, M., Duivenvoorden, J., Flenley, J., De Oliveira, P., van Geel, B., Graf, K., Gosling, W.D., Harbele, S., van der Hammen, T., Hansen, B., Horn, S., Kuhry, P., Ledru, M.-P., Mayle, F., Leyden, B., Lozano-García, S., Melief, A.M., Moreno, P., Moar, N.T., Prieto, A., van Reenen, G., Salgado-Labouriau, M., Schäbitz, F., Schreve-Brinkman, E.J., Wille, M., 2009. Pollen-based biome reconstructions for Latin America at 0, 6000 and 18 000 radiocarbon years ago. Clim. Past 5, 725–767. https://doi.org/10.5194/cp-5-725-2009, 2009.
Mason, C.C., Romans, B.W., Stockli, D.F., Mapes, R.W., Fildani, R., 2020. Detrital zircons reveal sea-level and hydroclimate controls on Amazon River to deep-sea fan sediment transfer. Geology 47, 563–567. https://doi.org/10.1130/G45852.1.
Melack, J.M., Hess, L.L., 2011. Remote sensing of the distribution and extent of wetlands in the Amazon Basin. In: Junk, W.J. (Ed.), Amazonian Floodplain Forests: Ecophysiology, Biodiversity and Sustainable Management, vol. 210. Ecological Studies, pp. 43–59. https://doi.org/10.1007/978-90-481-8725-6_2.
Molinari, R.L., Fine, R.A., Johns, E., 1992. The deep western boundary current in the tropical North Atlantic ocean. Deep-Sea Res. 39, 1967–1984. https://doi.org/10.1016/0198-0149(92)90008-H.
Mudelsee, M., Schulz, M., 1997. The Mid-Pleistocene climate transition: onset of 100 ka cycle lags ice volume build-up by 280 ka. Earth Planet Sci. Lett. 1, 117–123. https://doi.org/10.1016/S0012-821X(97)00114-3.
Murphy, B.P., Bowman, D.M.J.S., 2012. What controls the distribution of tropical forest and savanna? Ecol. Lett. 15, 748–758. https://doi.org/10.1111/j.1461-0248.2012.01771.x.
Musher, L.J., Giakoumis, M., Albert, J., Del-Rio, G., Rego, M., Thom, G., Aleixo, A., Ribas, C.C., Brumfield, R.T., Smith, B.T., Cracraft, J., 2022. River network rearrangements promote speciation in lowland Amazonian birds. Sci. Adv. 8, eabn1099. https://doi.org/10.1126/sciadv.abn1099.
Nilsson, J.A.U., Döös, K., Ruti, P.M., Artale, V., Coward, A., Brodeau, L., 2013. Observed and modeled global ocean turbulence regimes as deduced from surface trajectory data. J. Phys. Oceanogr. 43, 2249–2269. https://doi.org/10.1175/JPO-D-12-0193.1.
Oliveira, P.S., Marquis, R.J., 2002. The Cerrados of Brazil: Ecology and Natural History of a Neotropical Savanna. Columbia University Press, New York.
Oliveira, D., Sánchez-Goni, M.F., Naughton, F., Polanco-Martínez, J.M., Jimenez-Espejo, F.J., Grimalt, J.O., Martrat, B., Voelker, A.H.L., Trigo, R., Hodell, D., Abrantes, F., Desprat, S., 2017. Unexpected weak seasonal climate in the western Mediterranean region during MIS 31, a high-insolation forced interglacial. Quat. Sci. Rev. 161, 1–17. https://doi.org/10.1016/j.quascirev.2017.02.013.
Olson, D.M., Dinerstein, E., Wikramanayake, E.D., Burgess, N.D., Powell, G.V.N., Underwood, E.C., D'Amico, J.A., Itoua, I., Strand, H.E., Morrison, J.C., Loucks, C.J., Allnutt, T.F., Ricketts, T.H., Kura, Y., Lamoreux, J.F., Wettengel, W.W., Hedao, P., Kassem, K.R., 2001. Terrestrial ecoregions of the world: a new map of life on Earth. Bioscience 51, 933–938. https://doi.org/10.1641/0006-3568(2001)051[0933:TEOTWA]2.0.CO, 2.
Oksanen, F.J., Blanchet, F.G., Friendly, M., Kindt, R., Legendre, P., McGlinn, D., Minchin, P.R., O'Hara, R.B., Simpson, G.L., Solymos, P., Stevens, M.H., Szoecs, E., Wagner, H., 2019. Vegan: community ecology package. R package Version 2.4-3. https://CRAN.R-project.org/package=vegan.
Ortuño, T., Ledru, M.-P., Cheddadi, R., Kuentz, A., Favier, C., Beck, S., 2011. Modern pollen rain, vegetation and climate in Bolivian ecoregions. Rev. Palaeobot. Palynol. 165, 61–74. https://doi.org/10.1016/j.revpalbo.2011.02.004.
Pardoe, H.S., Cleal, J.C.J., Berry, C.M., Cascales-Miñana, B., Davis, B.A.S., Diez, J.B., Filipova-Marinova, M.V., Giesecke, T., Hilton, J., Ivanov, D., Kustatscher, E., Leroy, S.A.G., McElwain, J.C., Opluštil, S., Popa, M.E., Seyfullah, L.J., Stolle, E., Thomas, B.A., Uhl, D., 2021. Palaeobotanical experiences of plant diversity in deep time. II: how to measure and analyse past plant biodiversity. Palaeogeogr. Palaeoclimatol. Palaeoecol. 580, 110618. https://doi.org/10.1016/j.palaeo.2021.110618.
Pennington, R.T., Prado, D.E., Pendry, C.A., 2000. Neotropical seasonally dry forests and Quaternary vegetation changes. J. Biogeogr. 27, 261–273. https://doi.org/10.1046/j.1365-2699.2000.00397.x.
Pérez-Escobar, O.A., Zizka, A., Bermúdez, M.A., Meseguer, A.S., Condamine, F.L., Hoorn, C., Hooghiemstra, H., Pu, Y., Bogarín, D., Boschman, L.M., Pennington, R.T., Antonelli, A., Chomicki, A., 2021. The Andes through time: evolution and distribution of Andean floras. Trends Plant Sci. 27, 364–378. https://doi.org/10.1016/j.tplants.2021.09.010.
Peterson, R.G., Stramma, L., 1991. Upper-level circulation in the south Atlantic ocean. Prog. Oceanogr. 26, 1–73. https://doi.org/10.1016/0079-6611(91)90006-8.
Petschick, R., Kuhn, G., Gingele, F., 1996. Clay mineral distribution in surface sediments of the South Atlantic: sources, transport, and relation to oceanography. Mar. Geol. 130, 203–229. https://doi.org/10.1016/0025-3227(95)00148-4.
Piacsek, P., Behling, H., Ballalai, J.M., Nogueira, J., Venancio, I.M., Albuquerque, A.L.S., 2021. Reconstruction of vegetation and low latitude ocean-atmosphere dynamics of the past 130 kyr, based on South American montane pollen types. Global Planet. Change 201, 103477. https://doi.org/10.1016/j.gloplacha.2021.103477.
Pires, J.M., Prance, G.T., 1985. The vegetation types of the Brazilian Amazon. In: Prance, G.T., Lovejoy, T.E. (Eds.), Key Environments: Amazonia. Pergamon Press, pp. 109–145.
Pocknall, D.T., Wood, L.J., Geen, A.F., Harry, B.E., Hedlund, R.W., 2001. Integrated paleontological studies of Pliocene to Pleistocene deposits of the Orinoco delta, eastern Venezuela and trinidad. In: Goodman, D.K., Clark, R.T. (Eds.), Proceedings of the IX International Palynological Congress. American Association of Stratigraphic Palynologists Foundation, Houston, TX, pp. 319–326. USA 1996.
Poirier, R.K., Billups, K., 2014. The intensification of northern component deep water formation during the mid-Pleistocene climate transition. Paleoceanography 29, 1046–1061. https://doi.org/10.1002/2014PA002661.
Prentice, I.C., Cramer, W., Harrison, S.P., Leemans, R., Monserud, R.A., Solomon, A.M., 1992. A global biome model based on plant physiology and dominance, soil properties and climate. J. Biogeogr. 19, 117–134. https://doi.org/10.2307/2845499.
Prentice, C., Guiot, J., Huntley, B., Jolly, D., Cheddadi, R., 1996. Reconstructing biomes from palaeoecological data: a general method and its application to European pollen data at 0 and 6 ka. Clim. Dynam. 12, 185–194. https://doi.org/10.1007/BF00211617.
Pupim, F.N., Sawakuchi, A.O., Almeida, R.P., Ribas, C.C., Kern, A.K., Hartmann, G.A., Chiessi, C.M., Tamura, L.N., Minelo, T.D., Savian, J.F., Grohmann, C.H., Bertassoli Jr., D.J., Stern, A.G., Cruz, F.W., Cracraft, J., 2019. Chronology of Terra Firme formation in Amazonian lowlands reveals a dynamic Quaternary landscape. Quat. Sci. Rev. 210, 154–163. https://doi.org/10.1016/j.quascirev.2019.03.008.
R Core Team, 2020. R: A Language and Environment for Statistical Computing. R Foundation for Statistical Computing, Vienna, Austria. URL. https://www.R-project.org.
Reese, C.A., Liu, K.B., 2005. A modern pollen rain study from the central Andes region of South America. J. Biogeogr. 32, 709–718. https://doi.org/10.1111/j.1365-2699.2005.01.
Reis, L.S., Guimaraes, J.T.F., Souza-Filho, P.W.M., Sahoo, P.K., Figueiredo, M.M.J.C., Souza, E.B., Giannini, T.C., 2017. Environmental and vegetation changes in southeastern Amazonia during the late Pleistocene and Holocene. Quat. Int. 449, 83–105. https://doi.org/10.1016/j.quaint.2017.04.031.
Reis, L.S., Bouloubassi, I., Mendez-Millan, M., Guimarães, J.T.F., de Araújo Romeiro, L., Sahoo, P.K., Pessenda, L.C.R., 2022. Hydroclimate and vegetation changes in southeastern Amazonia over the past ~25,000 years. Quat. Sci. Rev. 284. https://doi.org/10.1016/j.quascirev.2022.107466.
Richardson, P.L., Fratantoni, D.M., 1999. Float trajectories in the deep western boundary current and deep equatorial jets of the tropical Atlantic. Deep-Sea Research II 46, 305–333. https://doi.org/10.1016/S0967-0645(98)00100-3.
Richardson, P.L., Hufford, G.E., Limeburner, R., Brown, W.S., 1994. North Brazil Current retroflection eddies. J. Geophys. Res. 99, 5081–5093. https://doi.org/10.1029/93JC03486.

Roubik, D.W., Moreno, P.J.E., 1991. Pollen and Spores of Barro Colorado Island. Missouri Botanical Garden, p. 268.
Rull, V., 2011. Neotropical biodiversity: timing and potential drivers. Trends Ecol. Evol. 26, 508–513. https://doi.org/10.1016/j.tree.2011.05.011.
Sato, H., Kelley, D.I., Mayor, S.J., Colvo, M.M., Cowling, S.A., Prentice, I.C., 2021. Dry corridors opened by fire and low CO_2 in Amazonian rainforest during the Last Glacial Maximum. Nat. Geosci. 14, 578–585. https://doi.org/10.1038/s41561-021-00777-2.
Scheff, J.S., Seager, R., Liu, H., Coates, S., 2017. No access are glacials dry? Consequences for paleoclimatology and for greenhouse warming. J. Clim. 30, 6593–6609. https://doi.org/10.7916/D8HH6XP8.
Silva, F.H.M., Santos, F.A.R., Lima, L.C.L., 2016. Flora Polínica das Caatingas: Estação Biológica de Canudos (Canudos, Bahia, Brasil). Feira de Santana, Micron, p. 120p.
Sousa, T.A., Venancio, I.M., Valeriano, C.M., Heilbron, M., Carneiro, M.T.W.D., Mane, M.A., Almeida, J.H., Smoak, J.M., Albuquerque, A.L.S., Silva-Filho, E.V., 2021. Changes in sedimentary provenance and climate off the coast of Northeast Brazil since the last Interglacial. Mar. Geol. 435, 106454. https://doi.org/10.1016/j.margeo.2021.106454.
Stockmarr, J., 1971. Tablets with spores used in absolute pollen analysis. Pollen Spores 13, 615–621.
Stramma, L., England, M., 1999. On the water masses and mean circulation of the South Atlantic Ocean. J. Geophys. Res. 104, 863–881.
Tarasov, P.E., Andreev, A.A., Anderson, P.M., Lozhkin, A.V., Leipe, C., Haltia, E., Nowaczyk, N.R., Wennrich, V., Brigham-Grette, J., Melles, M., 2013. A pollen-based biome reconstruction over the last 3.562 million years in the Far East Russian Arctic e new insights into climate-vegetation relationships at the regional scale. Clim. Past 9, 2759–2775. https://doi.org/10.5194/cp-9-2759–2013.
Teitler, L., Florindo, F., Warnke, D.A., Filippelli, G.M., Kupp, G., Taylor, B., 2015. Antarctic Ice Sheet response to a long warm interval across Marine Isotope Stage 31: a cross-latitudinal study of iceberg-rafted debris. Earth Planet Sci. Lett. 409, 109–119. https://doi.org/10.1016/j.epsl.2014.10.037.
Tian, F., Cao, X., Dallmeyer, A., Lohmann, G., Zhang, X., Ni, J., Andreev, A., Anderson, P., Anatoly, L., Bezrukova, E., Rudaya, N., Xu, Q., Herzschuh, U., 2018. Biome changes and their inferred climatic drivers in northern and eastern continental Asia at selected times since 40 cal ka bp. Veg. Hist. Archaeobotany 27, 1–15. https://doi.org/10.1007/s00334-017-0653-8.
Torres, V., Hooghiemstra, H., Lourens, L.J., Tzedakis, P.C., 2013. Astronomical tuning of long pollen records reveals the dynamic history of montane biomes and lake levels in the tropical high Andes during the Quaternary. Quat. Sci. Rev. 63, 59–72. https://doi.org/10.1016/j.quascirev.2012.11.004.
Traverse, A., 1988. Paleopalynology. Unwin Hyman, Boston, p. 600.
Tzedakis, P.C., Hooghiemstra, H., Pälike, H., 2006. The last 1.35 million years at Tenaghi Philippon: revised chronostratigraphy and long-term vegetation trends. Quat. Sci. Rev. 25, 3416–3430. https://doi.org/10.1016/j.quascirev.2006.09.002.
van der Hammen, T., 1974. The Pleistocene changes of vegetation and climate in tropical South America. J. Biogeogr. 1, 3–26. https://www.jstor.org/stable/3038066.
van der Hammen, T., Absy, M.L., 1994. Amazonia during the last glacial. Palaeogeogr. Palaeoclimatol. Palaeoecol. 109, 247–261. https://doi.org/10.1016/0031-0182(94)90178-3.
van der Hammen, T., Hoogiemstra, H., 2000. Neogene and Quaternary history of vegetation, climate, and plant diversity in Amazonia. Quat. Sci. Rev. 19, 725–742. https://doi.org/10.1016/S0277-3791(99)00024-4.
van Soelen, E.E., Kim, J.-H., Santos, R.V., Dantas, E.L., Almeida, F.V., Pires, J.P., Roddaz, M., Damste, J.S.S., 2017. A 30 Ma history of the Amazon River inferred from terrigenous sediments and organic matter on the Ceará Rise. Earth Planet Sci. Lett. 474, 40–48. https://doi.org/10.1016/j.epsl.2017.06.025.
Wade, B.S., Pearson, P.N., Berggren, W.A., Pälike, H., 2011. Review and revision of Cenozoic tropical planktonic foraminífera biostratigraphy and calibration to the geomagnetic polarity and astronomical time scale. Earth Sci. Rev. 104, 111–142. https://doi.org/10.1016/j.earscirev.2010.09.003.
Wang, X., Edwards, R.L., Auler, A.S., Cheng, H., Kong, X., Wang, Y., Cruz, F.W., Dorale, J.A., Chiand, H.-W., 2017. Hydroclimate changes across the Amazon lowlands over the past 45,000 years. Nature 541, 204–207. https://doi.org/10.1038/nature20787.
Weng, C., Bush, M.B., Chepstow-Lusty, A.J., 2004. Holocene changes of Andean alder (Alnus acuminata) in highland Ecuador and Peru. J. Quat. Sci. 19, 685–691. https://doi.org/10.1002/jqs.882.
Werneck, F.P., 2011. The diversification of eastern South American open vegetation biomes: historical biogeography and perspectives. Quat. Sci. Rev. 30, 1630–1648. https://doi.org/10.1016/j.quascirev.2011.03.009.
Wicaksono, C.Y., Aguirre-Guiterrez, J., Nouhra, E., Pastor, N., Raes, N., Pacheco, S., Geml, J., 2017. Contracting montane cloud forests: a case study of the Andean alder (*Alnus acuminata*) and associated fungi in the Yungas. Biotropica 49, 141–152. https://doi.org/10.1111/btp.12394.
Willeit, M., Ganopolski, A., Calov, R., Brovkin, V., 2019. Mid-Pleistocene transition in glacial cycles explained by declining CO_2 and regolith removal. Sci. Adv. 5, eaav7337. https://doi.org/10.1126/sciadv.aav7337.
Zhang, Y., Chiessi, C.M., Mulitza, S., Zabel, M., Trindade, R.I.F., Hollanda, M.H.B.M., Dantas, E.L., Govin, A., Tiedemann, R., Wefer, G., 2015. Origin of increased terrigenous supply to the NE SouthAmerican continental margin during Heinrich stadial 1 and the younger Dryas. Earth Planet Sci. Lett. 432, 493–500. https://doi.org/10.1016/j.epsl. 2015. 09.054.